

## **Distribution Agreement**

In presenting this thesis as a partial fulfillment of the requirements for a degree from Emory University, I hereby grant Emory University and its agents the non-exclusive license to archive, make accessible, and display my thesis in whole or in part in all forms of media, now or hereafter, including display on the World Wide Web. I understand that I may select some access restrictions as part of the online submission of this thesis. I retain all ownership rights to the copyright of the thesis. I also retain the right to use in future works (such as articles or books) all or part of this thesis.

Stefano Andre Martin

April 29, 2021

DNA Tether Assays and Flow Testing: Increasing Reproducibility and Throughput in Single Molecule Experiments

By

Stefano Andre Martin

Laura Finzi

Adviser

Department of Biology

Laura Finzi

Committee Member

David Dunlap

Committee Member

Nicole Gerardo

Committee Member

William Kelly

Committee Member

DNA Tether Assays and Flow Testing: Increasing Reproducibility and Throughput in Single  
Molecule Experiments

By

Stefano Andre Martin

Laura Finzi

Adviser

An abstract of  
a thesis submitted to the Faculty of Emory College of Arts and Sciences  
of Emory University in partial fulfillment  
of the requirements of the degree of  
Bachelor of Science with Honors

Department of Biology

2021

## Abstract

### DNA Tether Assays and Flow Testing: Increasing Reproducibility and Throughput in Single Molecule Experiments

By Stefano Andre Martin

DNA transcription essential to most, if not all cellular life. Transcription and gene expression are regulated by proteins called transcription factors, and DNA torsion and tension affect the binding and unbinding of transcription factors. Single molecule experiments allow us to study the mechanics of single molecules of DNA, something that is not possible under experimental conditions that hope to extract data from Avogadro's number scales. Techniques like tethered particle microscopy (TPM) and magnetic tweezers (MT) allow us to perform single molecule experiments and collect data, relying on DNA tether assays to perform experimentation. DNA tether assays involve anchoring a linear segment of DNA to an observation chamber and attaching the other end to a microscopic bead that can be manipulated and tracked. Some single molecule experiments, like the ones planned for the future in the Finzi lab, require multiple instances of buffer exchange within the chamber between data collection steps. This thesis shows a typical Magnetic Tweezer experiment and the limitations of the employed methods for tether assay assembly and manipulation. This thesis also describes the development of a pump-assisted flushing system and corresponding software to extract data stored in video formats. The ability of a construct of DNA to stretch, twist, and be inducible to supercoiling was tested and the construct was used in further testing with the aim of mitigating the adverse effects of uncontrolled and non-reproducible fluid exchange rates within the observation chambers.

DNA Tether Assays and Flow Testing: Increasing Reproducibility and Throughput in Single  
Molecule Experiments

By

Stefano Andre Martin

Laura Finzi

Adviser

A thesis submitted to the Faculty of Emory College of Arts and Sciences  
of Emory University in partial fulfillment  
of the requirements of the degree of  
Bachelor of Science with Honors

Department of Biology

2021

## Acknowledgements

Great many thanks to Laura Finzi and David Dunlap for giving me the opportunity to work directly in the study of life and making this research possible. I would like to thank Nicole Gerardo for her continued support and guidance throughout my time at the college, and I would like to thank William Kelly for his support and for reminding me how much fun it can be learning about the processes of life.

My greatest thanks I give to my mother, Olga Moreno, my father, Humberto Martin, and my brother, Mihael Martin, for their unwavering love and support throughout my life.

## Table of Contents:

- I. Chapter I: Introduction
  - A. The Central Dogma and DNA
  - B. DNA Topology and Supercoiling
  - C. Single Molecule Experiments and DNA Tether Assays
  - D. Experimental Goals and Significance
- II. Chapter II: Experimental Planning
  - A. Tether Preparation
  - B. Flow Chamber Preparation
  - C. Tethered Particle Tracking and Magnetic Tweezers
  - D. Flow Tests: Bulk Flow & Bead Displacement Tracking
- III. Chapter III: Results
  - A. Magnetic Tweezer Tests
  - B. Flow Tests using Tissues and Micropipettes
  - C. Flow Tests with Pump Implementation
- IV. Chapter IV: Discussion
  - A. Making A New DNA Tether for MT Measurements of Protein-Constrained Torsion
  - B. Implementation of a Pump Flow System for Reproducible Chamber Preparations
  - C. Future Objectives and Outlook
- V. References
- VI. Appendix
  - A. pDD\_1N3BbvCI Plasmid and Primer Sequences
  - B. Video Player MATLAB Code
  - C. Flow Chamber Assembly Protocols
  - D. Calibration Slide and Pixel Conversion Factor

Table of Figures:

**Figure 1.** Chemical Structures of Nucleic Acid Monomers and Base Pairing.

**Figure 2.** DNA Structure and Central Dogma

**Figure 3.** Histone-DNA Complex and Lac Repressor

**Figure 4.** Plectonemic DNA Supercoiling

**Figure 5.** Polymerase Chain Reaction

**Figure 6.** Restriction Endonuclease and Ligation Reaction

**Figure 7.** Agarose Gel Electrophoresis

**Figure 8.** pDD\_1N3BbvCI Plasmid and DNA Tether Fragment PCR Results

**Figure 9.** Fragment Ligation and Gel Confirmation

**Figure 10.** Model Cross-Section of a Flow Chamber

**Figure 11.** Diagram of  $B$  Induced Forces on Beads

**Figure 12.** Magnetic Tweezer Microscope

**Figure 13.** Leica Light Microscope (LM) and Pump System

**Figure 14.** Custom Video Player GUI

**Figure 15.** Magnetic Tweezing Experiments and Sample Field of View

**Figure 16.** Micropipette-Tissue Sample Loading Strategy

**Figure 17.** Flow Chamber and Slide Adapter Design

**Figure 18.** Bead Average Velocities vs Buffer Exchange Strategy

## **Chapter I: Introduction**

### The Central Dogma and DNA

The mid to late twentieth century ushered new discoveries which exponentially increased the understanding of the principles responsible for dictating the order, structure, and function of the natural world and its organisms. The work of Edwin Chargaff, Rosalind Franklin, James Watson, and Francis Crick and others<sup>3</sup> demonstrated the structure of the deoxyribonucleic acids (DNA) and its function as the seemingly universal genetic code.<sup>10</sup> (*Lehninger et al.*, 288) Richard Dawkins projected these findings from an evolutionary perspective, showing that selective pressures influence the maintenance and transmission of genes.<sup>5</sup>

Decades of research led to the development and eventual acceptance of the Central Dogma of biology, which describes the transfer of sequential information encoded in biopolymers from DNA to ribonucleic acids (RNA), and finally proteins.<sup>10</sup> (*Lehninger et al.*, 977) The sequential order of the bases Adenine (A), Thymine (T), Cytosine (C), and Guanine (G) (Figure 1A) within a DNA molecule dictates the nucleotide sequence of a corresponding messenger RNA (mRNA) synthesized by RNA polymerase (Figure 1C). The mature messenger RNA (mRNA) is then translated by ribosomes directly, or after a series of modifications involving RNA splicing and the removal of introns in eukaryotes.<sup>10,24</sup> The amino acid sequence of the mRNA determines both the structure and function of the resultant translated protein.<sup>3,10,24</sup> Figure 2 is an illustration of these processes.

A strand of DNA is composed of a series of covalently linked deoxynucleotide monomers. Each monomer consists of a deoxyribose 5-member sugar ring, an inorganic phosphate residue, and a corresponding nucleoside base (Figure 2A).<sup>11,25,29</sup> A single strand of DNA (ssDNA) is developed

as the 5' carbon of the deoxyribose ring of one monomer forms a phosphodiester linkage with the 3' hydroxyl group of the subsequent monomer. However, usually, DNA exists in a double stranded (dsDNA) conformation, with the two complementary strands in an antiparallel conformation (Figure 2B). Base pairs are located between the sugar-phosphate backbones, C forming three hydrogen bonds with G, and A, two bonds with T (Figure 1D&E Figure 2A). DNA can take many different conformations, but the double-stranded, right-handed B conformation is the one most commonly referred to, as it is the conformation that DNA adopts in aqueous physiological saline environments.<sup>11,29</sup> DNA has a *helical pitch* ( $p$ ) close to 10.5 bp and a diameter of about 2 nm, with major and minor groove widths of approximately 2.2 nm and 1.2 nm, respectively.<sup>10,24,28</sup>

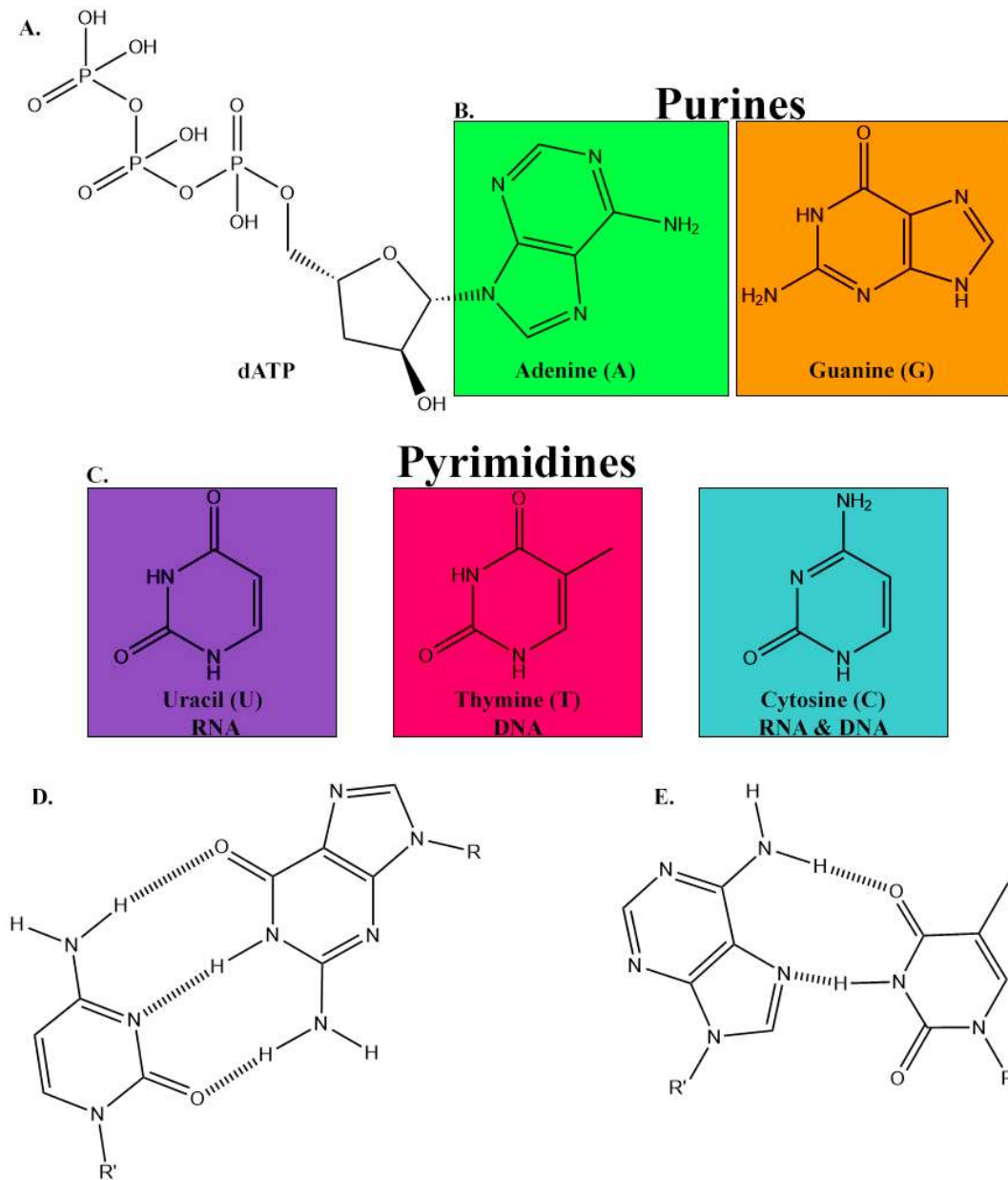


**Figure 1.** Chemical Structures of Nucleic Acid Monomers and Base Pairing. **A.** Chemical structure of deoxyadenosine triphosphate. dATP is a substrate of DNA polymerase. It is used in PCR in conjunction with other deoxynucleotide triphosphate substrates (dNTPs). **B.** Chemical structure of adenine and guanine, the purine bases. Both are included in DNA and RNA biopolymers. **C.** Chemical structures of pyrimidine bases uracil, thymine, cytosine from left to right. Cytosine is incorporated into both DNA and RNA biopolymers, while thymine and uracil are generally only incorporated into DNA and RNA, respectively.<sup>10</sup> **D.** Visual representation of the hydrogen bonding between guanine and cytosine, located on the interior of the B-DNA double helix (not shown). **E.** Visual representation of the double bonding between adenine and thymine.

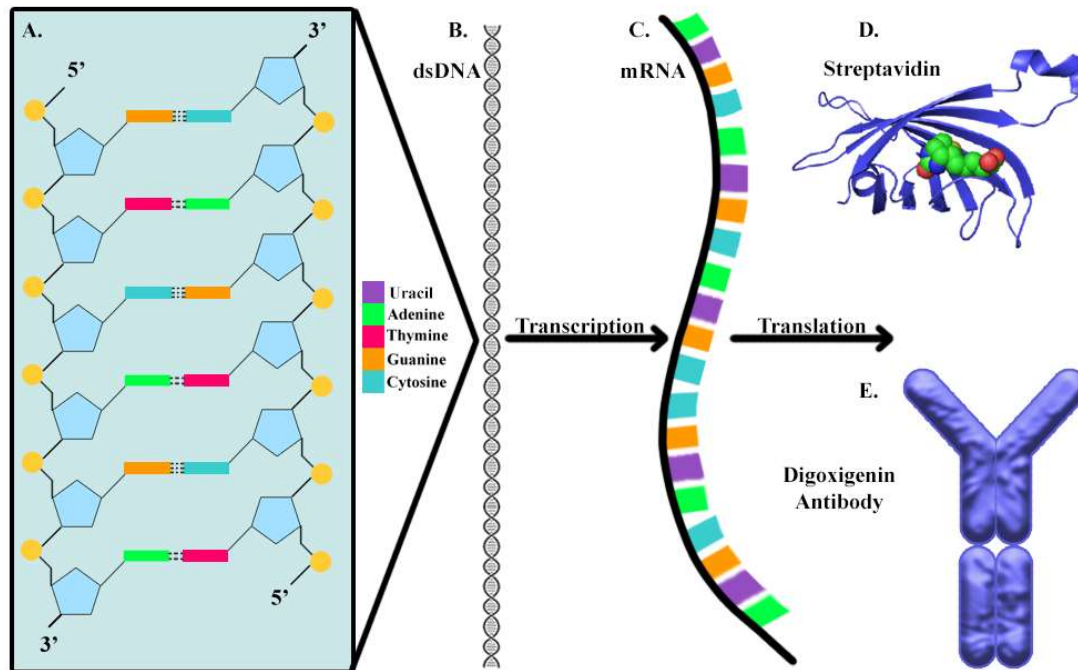


**Figure 2.** DNA Structure and Central Dogma **A.** Diagram of the secondary structure of a dsDNA molecule. Blue pentagons represent deoxyribose sugars, yellow dots represent inorganic phosphate residues, and the colored boxes represent nucleoside bases, per the key in the figure. **B.** Diagram of the tertiary structure of dsDNA. The genetic code stored in DNA is transcribed into RNA, per the central dogma. **C.** Diagram of the secondary structure of RNA. Purple boxes represent uracil bases, as thymine is not generally present in RNA. The genetic code carried by mRNA polymers is translated into proteins. **D.** Ribbon diagram of a streptavidin monomer (protein), isolated from the bacterium *Streptomyces avidinii*. The monomers associate to form a tetramer (not shown) with extremely high binding affinity for biotin makes it perfect for tether construction. **E.** Diagram of a digoxigenin antibody (antidigoxigenin), used to functionalize the glass of flow chambers due to its affinity to digoxigenin.

### DNA Topology and Supercoiling

The topology of DNA is modified by proteins that bind to it. Arguably, the most well-known example of proteins modifying DNA topology lies with eukaryotic histones: arginine and lysine rich proteins with positive charges.<sup>10</sup> (*Lehninger et al, 1995*) These proteins form a cylindrical complex, the histone octamer, which DNA wraps around, creating what is known as a nucleosome (Figure 3A). The “beads on a string”-like conformation (Figure 3B) is compacted into a 30 nm structure (Figure 3C), followed by further arrangement into more complex structures until final compaction into chromosomes.<sup>10,24</sup> Nucleosomes are an example of protein-

constrained DNA supercoiling since the DNA forms one and one half left-handed superhelical turns around the histone octamer. Histones, however, are not the only DNA associating proteins that alter its topology. Many transcription factors (TFs) have been shown to cause topological changes to the DNA upon binding like bending, looping, warping, and wrapping. One example of this is the lac repressor, which binds at two distant, specific sites on the DNA and induces looping (Figure 3D).<sup>11,29</sup> The DNA loop increases repression of the lac operon in the bacterium *E. coli* when there is no need to express the proteins responsible for the metabolism of lactose, such as in the absence of lactose. The topological changes to DNA molecules induced by these DNA-binding proteins directly affect gene expression and regulation.

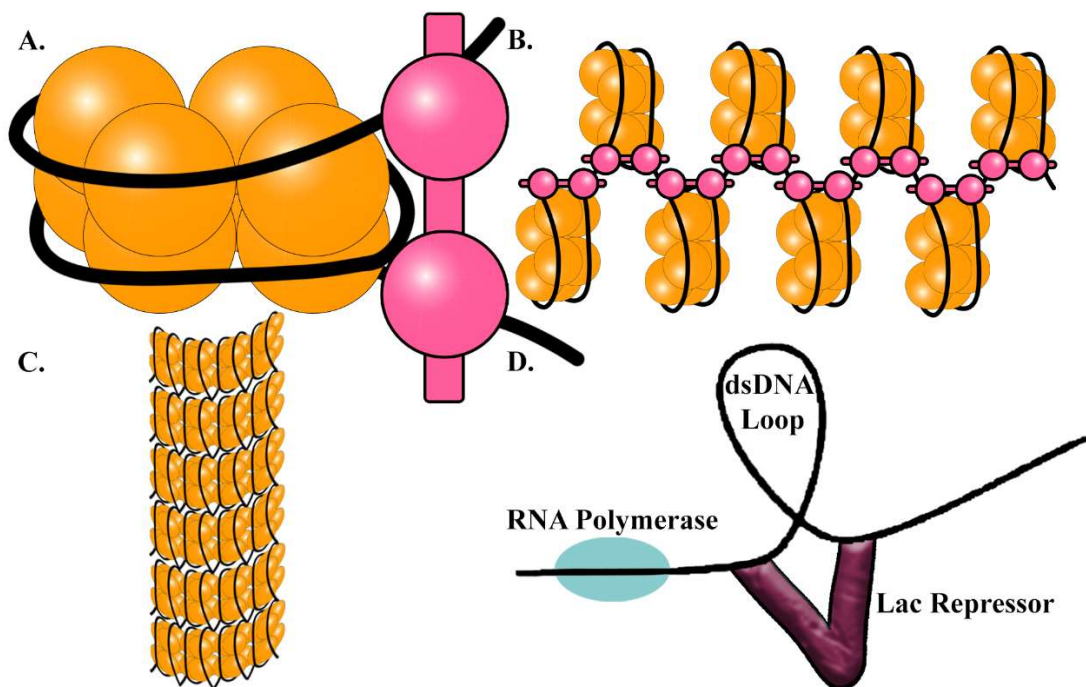


**Figure 3.** Histone-DNA Complex and Lac Repressor. **A.** Diagram of a nucleosome. Individual assorted histone monomers (yellow) associate to form an octamer, which acts as a spool for dsDNA (black) to wind around. Histone H1 (Pink) binds to the entry and exit sites of the nucleosome. **B.** Diagram of the “beads on a string” structure formed by repeating nucleosome cores on the same segment of DNA. **C.** Diagram of the 30 nm fiber. **D.** Diagram showing the binding of the lac repressor (maroon) to two different recognition sites on a dsDNA, inducing loop formation. The loop increases the repression of the lac operon in *E. coli*.

In order to understand and quantitatively treat DNA supercoiling, the *linking number* ( $Lk$ ), is defined as the number of times that one of the DNA strands crosses the other. Linking number is calculated by dividing the number of base pairs  $n$  by the helical pitch  $p$  (10.5 bp):

$$Lk_0 = n/p \quad (1)$$

The change in linking number, due to winding or unwinding of the strands, can be defined as:

$$\Delta Lk = Lk - Lk_0 \quad (2)$$

where  $Lk_0$  is the linking number of the relaxed and unconstrained molecule, and  $Lk$  is the final linking number. Often  $\Delta Lk$  is expressed as a percentage, in a quantity known as superhelical density ( $\sigma$ ):

$$\sigma = \Delta Lk/Lk_0 \quad (3)$$

This quantity indicates by how much a torsionally constrained DNA molecule deviates from its torsionally relaxed state. James White deduced that the linking number for a string torsionally constrained in three dimensions is invariable under non-degenerate isotopy.<sup>31</sup> The same principle applies to the case of torsionally constrained dsDNA, as long as the strands are not nicked.

White's theorem expresses the linking number of as:

$$Lk = Tw + Wr \quad (4)$$

where  $Lk$  can be separated into two different structural components twist ( $Tw$ ) and writhe ( $Wr$ ). In the case of DNA,  $Tw$  refers to the actual twisting of the molecule, or the number of its helical turns, and  $Wr$  to the number of times both strands of double helix cross over themselves (Figure 4). Therefore,  $Wr$  is a measure of the coiling of the double-stranded molecule on itself. For a

torsionally relaxed dsDNA, the linking number  $Lk_0$  is constant, and the segment has no writhe ( $Wr_0 = 0$ ). Therefore, given equations 1 and 4, one can calculate:

$$Lk_0 = Tw_0 = n/p \tag{5}$$

Supercoiled DNA is understood to have

$$\Delta Lk \neq 0 \text{ or } \sigma \neq 0 \tag{6}$$

Different supercoiling conformations exist, and White's theorem facilitates their classification. Since topological changes to DNA structure serve important regulatory functions, *in vitro* methods have been developed to facilitate the visualization and study of molecular response to torsion.<sup>16</sup>

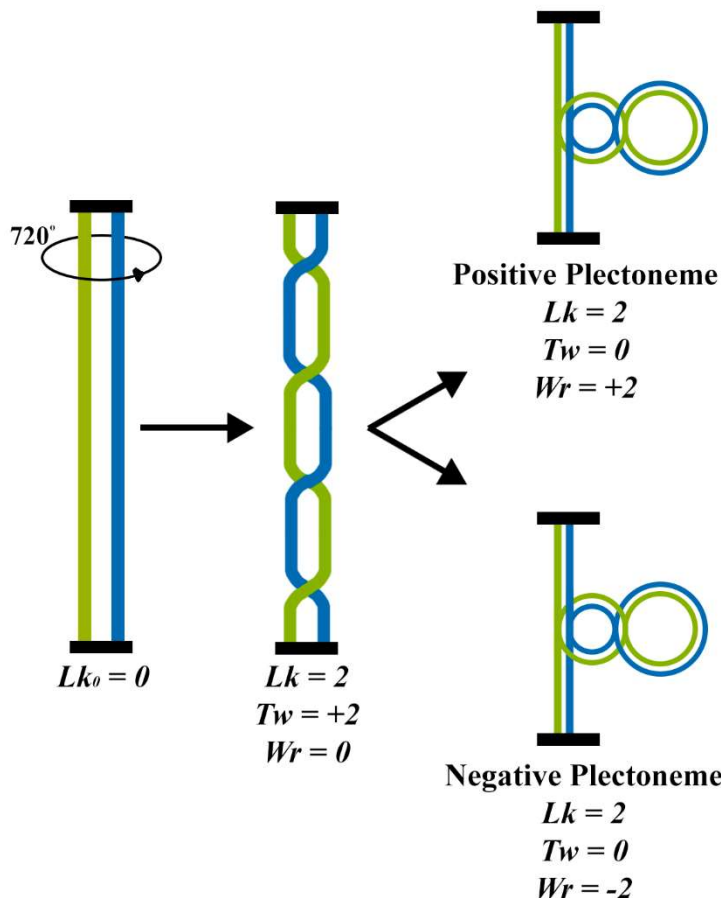


**Figure 4. Plectonemic DNA Supercoiling Characterization.** A right-handed dsDNA molecule can be characterized by its *linking number*  $Lk$ , *twist*  $Tw$ , and *writhe*  $Wr$ . In order to simplify visualization of supercoiling, dsDNA is represented here as a pair of parallel strings. Fixing one end of the system while rotating the other end twice over itself increases  $Lk$  by 2. The increase in linking number induces supercoiling of the DNA molecule into structures called plectonemes. Depending on the direction of twisting, negative and positive supercoiling can occur.

### Single Molecule Experiments and DNA Tether Assays

Single molecule experiments, as their name suggests, provide the means to quantitatively measure the behavior of individual molecules. *In vitro* single molecule manipulation techniques are very powerful as they facilitate the collection of data regarding the structure and kinetics of DNA, even in the presence of transcription factors or other DNA-associating proteins, without population averaging. The fact that measurements can be taken from single molecules presents a distinctive advantage over bulk experimental methods that attempt to interpret data obtained from samples containing Avogadro numbers of molecules, conditions which are liable to obscuring interactions due to ensemble averaging.<sup>1,6,19</sup>

There are currently a number of different single molecule techniques, including atomic force microscopy (AFM), tethered particle microscopy (TPM), and magnetic tweezers (MT), with the latter two techniques employing DNA tether assays. DNA tether assays involve attaching a microscopic bead to the end of a linear of DNA molecule, while attaching the other of the DNA molecule to the surface of a flow chamber. The flow chamber allows for buffer exchange and microscope visualization. Even though the DNA molecule is not observed directly, the bead that is attached to it is. While the bead is subject to thermal Brownian diffusion, its range of motion is constrained by the DNA tether to which it is attached to an extent determined by the length of the tether. The motion of the bead is recorded as a function of time, which can be used to calculate the effective length of the DNA tether.<sup>6,7,12,18,27</sup>

For measurements involving the application of tension, the worm-like chain model used to describe the elastic behavior of DNA.<sup>1,25</sup> The model assumes that the dsDNA molecule is a homogenous, continuously flexible rod-like polymer with a characteristic persistence length, a property that quantifies a polymer's bending stiffness.<sup>1,27</sup>

### Experimental Goals and Significance

The goal of this project was to find a way to abruptly release the torsional constraint on a DNA tether in a magnetic tweezer set-up. This was part of a larger study on the effect of supercoiling on DNA. Originally, we hoped to do this by introducing a nicking enzyme into the flow chamber during particle tracking. Reproducible preparation of DNA tethered beads in a flow chamber proved to be a major complication however, so I began to concentrate on establishing reliable methods for sample preparation.

## **Chapter II: Experimental Planning**

### Tether Preparation

DNA tethers were prepared using a combination of different, well documented techniques. These included amplification via polymerase chain reaction (PCR), site-specific enzymatic restriction and ligation, and agarose gel electrophoresis. PCR amplifies minimal quantities of DNA into much greater and usable quantities using a thermocycler to program multiple rounds of DNA replication. In order to do so, a sample of DNA must be combined with an abundance of primers, sufficient Taq DNA polymerase (derived from *Thermus aquaticus*), dNTPs (for chemical structure of dATP see Figure 1A), and buffer. First, the sample of dsDNA is heated to a high enough temperature, approximately 95 °C, to disrupt the hydrogen bonds between the complementary base pairs of the double helix. This disruption of the hydrogen bonding causes the individual strands to dissociate, yielding two complementary single strands of DNA (ssDNA). Once separated, the temperature is lowered considerably to between 50-55 °C, allowing the oligonucleotide primers to anneal to complementary sequences in the ssDNA template. The molar concentration of the oligonucleotide primers is so much greater than that of the sample DNA that they anneal much more readily to the ssDNA template than the complementary ssDNA. After the annealing step, the temperature is raised once more during the elongation step to about 72 °C. The increase in temperature activates the Taq polymerase, allowing it to begin replication of the template strand starting from the oligonucleotide primer, in the 5' to 3' direction. This results in two daughter dsDNA strands each containing a single parent strand. These steps are repeated at least thirty times, yielding exponentially greater amounts of amplicon than originally started with.<sup>20,24</sup> A graphical description of PCR is provided in Figure 5.

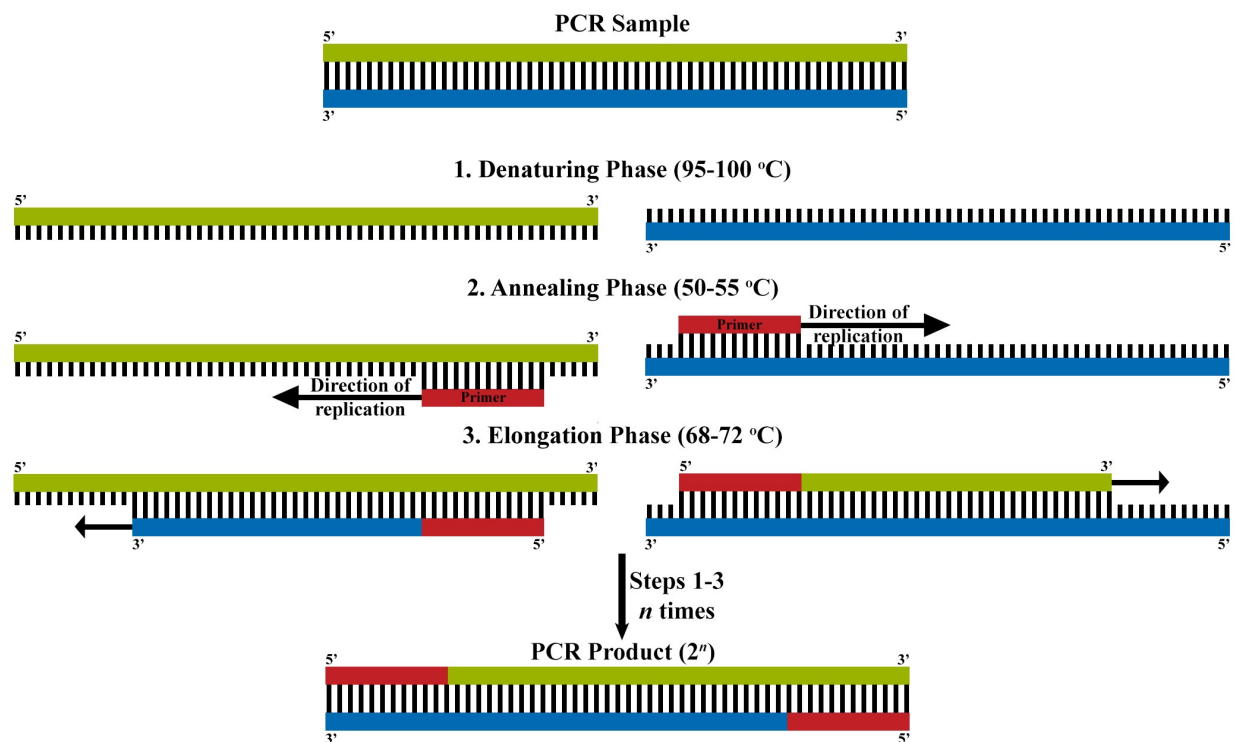


**Figure 5.** Polymerase Chain Reaction. Sample dsDNA is placed in solution along with excess oligonucleotide primers, dNTPs, DNA polymerase and polymerase buffer. Using a thermocycler, the solution temperature is fluctuated between steps 1-3 as described above. Denaturation phase (1) raises the temperature to cause strand separation. Lower annealing phase (2) temperatures allow oligonucleotide primers to associate with the complementary sequences on each strand. Arrows in this step only demonstrate the future direction of replication. During the elongation phase (3) DNA polymerase (not pictured) incorporates individual dNTPs to extend primers until synthesis of the new daughter strand is complete. Steps 1-3 are repeated anywhere between 30-40 times, exponentially increasing the number of copies of sample DNA.

Enzymatic cleavage and ligation (Figure 6) also form an integral part of the process of tether preparation. Restriction enzymes have been shown to recognize specific DNA sequences, known as restriction sites, where they associate and cleave the DNA's phosphodiester backbone at a specified distance, with cuts producing either "blunt" or overhanging "sticky" ends, depending on the enzyme class.<sup>9</sup> Figures 6 A and B illustrate the cleavage of dsDNA by two restriction enzymes that produce sticky ends. Type I restriction endonucleases are known to cleave DNA at

random sites that can be over 1,000 base pairs away from the recognition site, while type III will generally cleave DNA at positions 25 base pairs away from the recognition site.<sup>10,24</sup> Type II restriction endonucleases were used in this experiment in favor of the others, as these enzymes are not ATP-dependent and will catalyze enzymatic cleavage at recognition sequences of about 4 to 6 base pairs long.<sup>9,10,24</sup> Restriction enzymes that produce overhanging sticky ends were used in this experiment because the sticky ends facilitate the ligation of complementary sequences, allowing the purposeful combination of different fragments of DNA. The ligation of complementary sequences of the overhanging ends is performed by a class of enzymes known as ligases, which reestablish the phosphodiester linkages of the backbone.

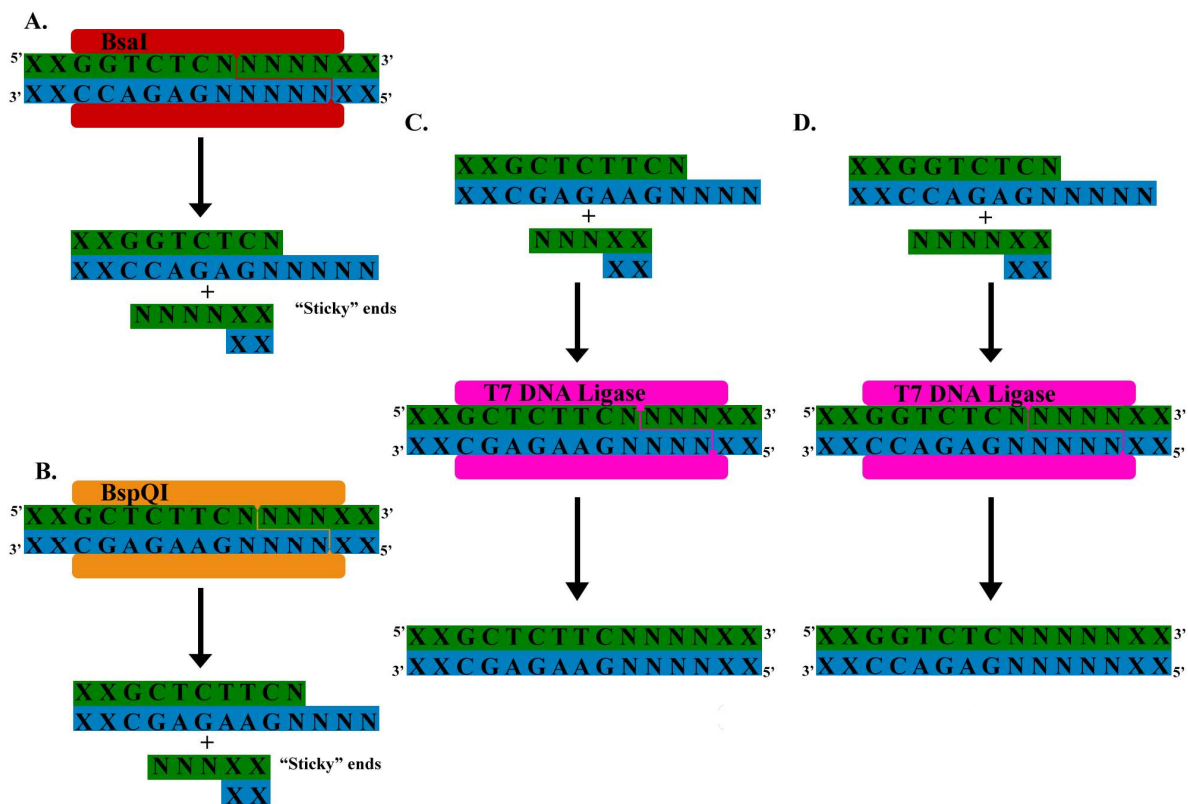


**Figure 6.** Restriction Endonuclease and Ligation Reaction. **A.** Visual representation of restriction endonuclease BsaI cleaving dsDNA at the enzyme's corresponding recognition site and producing sticky ends. **B.** BspQI cleaving dsDNA at the enzyme's corresponding recognition site, also producing sticky ends. **C.** T7 DNA Ligase re-establishing phosphodiester linkage of DNA sections with corresponding overhanging ends. Here T7 ligase is ligating at the BspQI recognition site. **D.** Same as C. but T7 ligase is ligating at the BsaI recognition site.

Gel electrophoresis was applied at multiple stages, as it verifies the success and accuracy of ligation and restriction reactions, as well as the products of PCR reactions. Given that DNA has a net negative charge owing to the phosphate moieties in the backbone, when placed in an electric field DNA will be attracted to the positive pole. The best way to achieve this is to load DNA inside an agarose gel which provides a matrix within which it can migrate under the influence of an electric field. Indeed, when agarose is combined with water, heated, and then allowed to cool, it forms a hydrogel with pores the size of a few nanometers, through which the DNA can move. Not all DNA is of equal size, however, and the longer a DNA is, the more difficulty the molecule will encounter sieving through the gel. Conversely, smaller DNA fragments traverse the gel matrix more easily, so they travel faster than do larger fragments. The separation according to length of different DNA fragments in an agarose gel yields “bands” of DNA at different distances from the well.<sup>24</sup> These bands can be observed under ultraviolet light ( $\lambda = 302$  nm). Stock solutions of DNA “ladders” are commercially available, and when ran on the gel alongside the samples, producing a calibrated band pattern that can be used to approximate the sizes of sample DNA segments based on their positions in comparison to the respective bands from the ladder. A graphic of gel electrophoresis is available for reference in Figure 7.

For TPM measurements, anchorage to the antidigoxigenin-coated flow chamber surface and streptavidin-coated bead labeling of single DNA molecules is achieved by ordering primers that are labeled either with a digoxigenin or a biotin. However, for most magnetic tweezer experiments where DNA needs to be twisted, the main DNA fragment needs to be attached to the flow chamber surface and bead via multiple linkages. This is achieved by synthesizing a biotin-labeled “bio” and a digoxigenin-labeled “dig” DNA tether fragment “tail” via PCR (Figure 8), which are then ligated to an unlabeled main fragment (Figure 9).

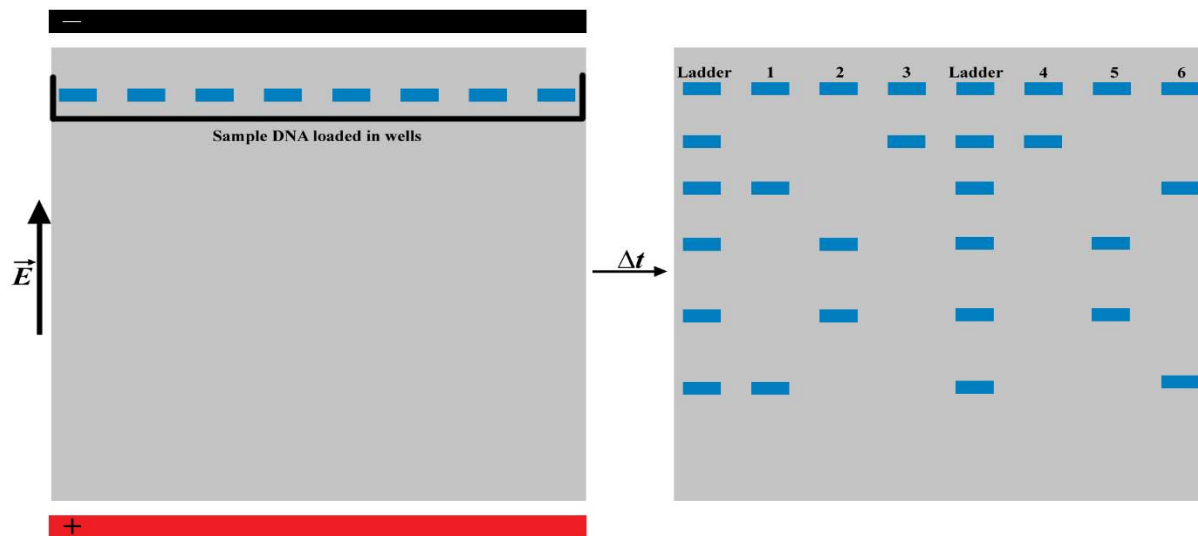


**Figure 7.** Agarose Gel Electrophoresis. Visual description of the process of agarose gel electrophoresis. DNA is loaded into wells in the agarose gel and the gel is placed in an electric field for a certain amount of time. After the time passes, the DNA has segregated into different bands according to size, which can be referenced to the DNA ladders that ran alongside the samples.

Here, a customized plasmid (pDD\_1N3BbvCI) was propagated in *Escherichia coli* and was used to create the bio- and dig-tails, along with the main fragment to which the tails anneal. Different aliquots of the plasmid were used to amplify the different sections of the plasmid, using different primer pairs as well. PCR spiked with biotin or digoxigenin-labeled deoxy-uracil triphosphate (dUTPs) was performed to amplify the biotin-labeled and digoxigenin-labeled tails, respectively. This resulted in functionalization of the DNA segments along multiple random positions in the sequence where a labeled uracil residue was incorporated in place of thymine. Verification of proper amplification was performed via agarose gel electrophoresis, and a visual overview of the process of fragment synthesis is provided in Figure 8.

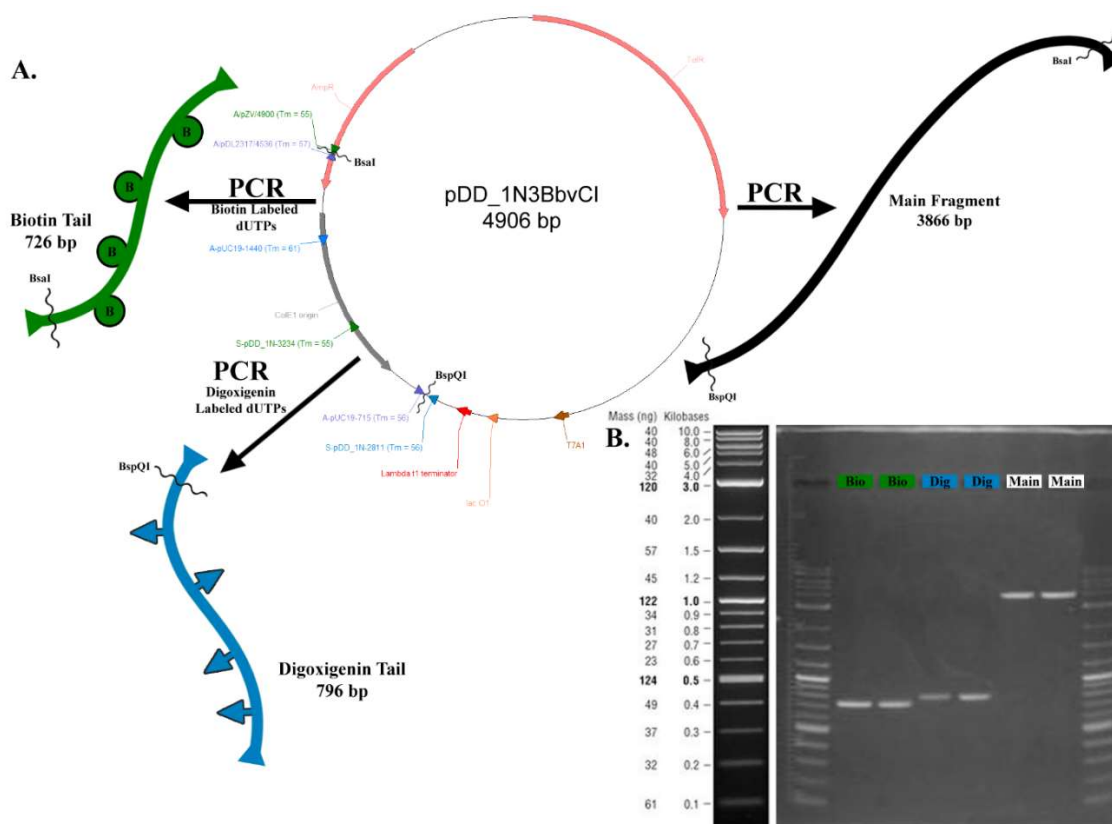


**Figure 8.** pDD\_1N3BbvCI Plasmid and DNA Tether Fragment PCR Results. **A.** Map of the pDD\_1N3BbvCI plasmid and visualization of the process required to amplify sections of the plasmid. Tether fragments (“tails”) functionalized with biotin were prepared by PCR, using biotin-labeled dUTPs and primers A/pZV/4900 and S-pDD\_1N-3234. Tails functionalized with digoxigenin were prepared by PCR using digoxigenin-labeled dUTPs and primers A-pUC19-1440 and S-pDD\_1N-2811. Main fragments were prepared using unlabeled dNTPs and primers A/pDL/2317/4536 and A-pUC19-715. Digestion by corresponding restriction enzymes is performed following verification of PCR (not shown). **B.** Gel electrophoresis results confirming proper PCR amplification. Bands are identified according to the specified sequence lengths in *B.* by cross-referencing the band’s position relative to the ladder (lanes 1 and 8).

Once all the necessary DNA fragments were prepared, they were combined via ligation paired with restriction enzyme digestion. The enzymes used for restriction were BsaI and BspQI (New England Biolabs “NEB” Ipswich, MA), and T7 DNA ligase (NEB) was used to combine the fragments (Figures 7 and 9). Once ligated, the tethers are incubated with superparamagnetic beads, in the case of magnetic tweezers, coated with streptavidin tetramers. The streptavidin

tetramers have very high binding affinities (with a strength comparable to that of a covalent bond) for the biotin moieties located on the bio-tails.<sup>8,21,22</sup>

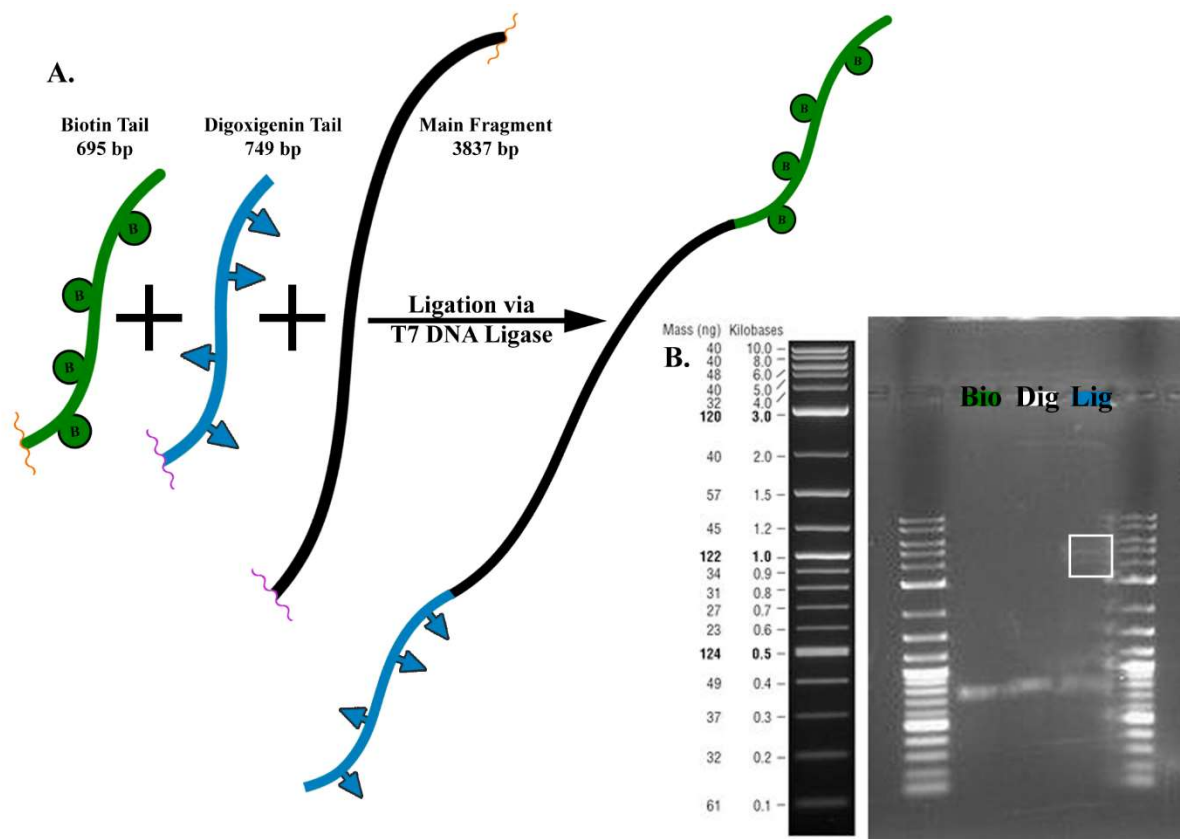


**Figure 9.** Fragment Ligation and Gel Confirmation. **A.** Graphic summary of the ligation between the two functionalized tail fragments and the main fragment. At this point, all tether fragments have been digested by BsaI (yellow), BspQI (purple), or both restriction endonucleases. T7 DNA ligase will reinstate the phosphodiester bond on the sugar-phosphate backbone of annealing complementary sticky ends of different tether segments. **B.** Gel electrophoresis results confirming the proper ligation of the different tether segments to create the DNA tether complex. There is a faint band between 5,000 and 6,000 bp where properly ligated tethers would be expected (5,281 bp). Other bands present in the ligation well represent unused reagents.

### Flow Chamber Preparation

The protocol for flow chamber preparation varies somewhat between instruments, experiment, and operator. Thus, a more reproducible protocol and design for flow chamber preparation became a goal of this research.

Flow chambers (Figure 10) are prepared by placing a parafilm gasket, cut to shape by a laser cutter, between two pieces of thoroughly cleaned glass. Glass is washed for at least 60 minutes in lab soap and water on an orbital shaker, rinsed copiously with water, then distilled water, and stored under 99% ethanol. The flow chamber is heated on a hot plate at low temperatures, causing the parafilm to melt slightly and adhere to the two glass surfaces and creating a watertight seal. A combination of buffers that include phosphate buffered saline (PBS), bead wash buffer (BWB), tethered bead buffer (TBB), and stretching buffer (SB) were used in the preparation of flow chambers (see below for buffer composition). PBS at pH 7.4 has a similar osmolarity and pH to that of extracellular fluid.<sup>14</sup> As the name suggests, BWB is used to wash beads that are taken from the stock solution, as they tend to aggregate. It is composed of a combination of 1 M NaCl, 10 mM Tris-HCl, and 1 mM ethylenediaminetetraacetic acid (EDTA), where Tris-HCl is used as a pH buffer while EDTA removes metal ions, preventing endonuclease activity that requires divalent metal ions in solution.<sup>2</sup> TBB is composed of 100 mM NaCl, 20 mM Tris-HCl, and 1 mM EDTA and is used for chamber flushing during functionalization. SB is a combination of 100 mM NaCl, 0.2 mg/ml casein, 2 mM EDTA, and Tween in 20 mM Tris-HCl at a 0.5% volume to volume ratio, where Casein prevents nonspecific association of other proteins with DNA,<sup>17</sup> and Tween improves antigen-antibody association.<sup>32</sup>

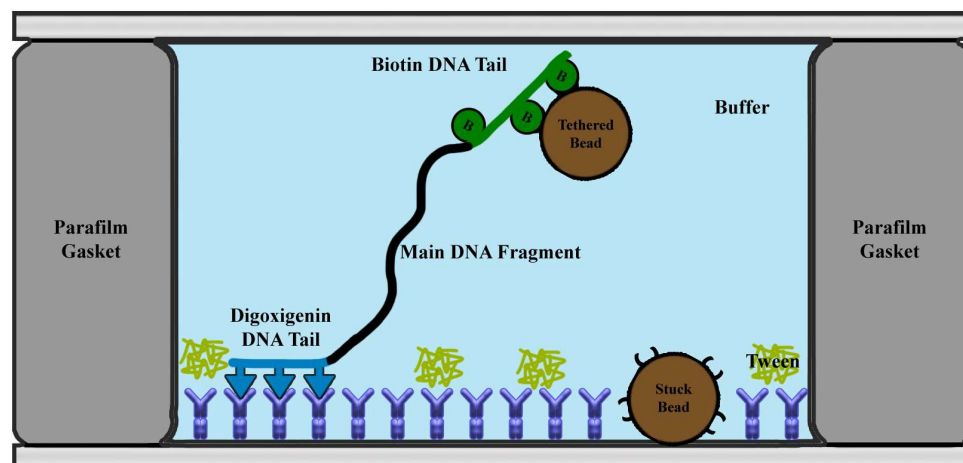


**Figure 10.** Model Cross-Section of a Flow Chamber. Flow chambers are used to make DNA tether assays for single molecule experiments. The digoxigenin moieties (blue arrows) on the dig-tail associate with the anti-digoxigenin

(purple Ys) on the glass surface. The flow chamber is filled with solution and the bead undergoes thermal Brownian diffusion with its range of motion constrained by the nucleic acid it is attached to.

The chamber is initially flushed with PBS and incubated at room temperature with 4  $\mu\text{g/ml}$  antidigoxigenin (Roche, Madison, WI) in PBS for at least one hour, but no more than two. Following the incubation, the chamber is rinsed with TBB. A small aliquot of superparamagnetic beads (Dynabead MyOne Streptavidin T1, Invitrogen, Life Technologies, Grand Island, NY) from the stock solution is washed in BWB using a rare earth magnet and lab-top vortexer, then suspended in TBB. Washed beads are subsequently introduced into an aliquot of DNA tethers, also suspended in TBB, and after a short incubation period the bead-DNA tether complex is introduced into the flow chamber. At this point, the digoxigenin moieties on the dig-tail associate with the anti-digoxigenin (immunoglobulin antibodies) attached to the functionalized glass surface of the flow chamber.<sup>26</sup> After a few minutes, the chamber is then flushed with SB and placed under the microscope for observation. A model cross section of the flow chamber is provided for reference in Figure 10, and the complete protocol for assembly is provided in Appendix C.

### Tethered Particle Tracking and Magnetic Tweezers

The tethered particle motion (TPM) technique consists in monitoring the Brownian motion of beads tethered to the glass surface of a microscope flow chamber by single DNA molecules using optical microscopy.<sup>30</sup> No force field is present. Magnetic tweezers (MT) instead rely on the magnetic field generated by a couple of permanent magnets placed above the stage of an optical microscope for rotating and pulling superparamagnetic beads tethered to the surface by single DNA molecules (Figure 11A). Therefore, MT allow manipulation of individual DNA molecules which can be twisted and stretched on command.<sup>16,29</sup> As the magnet's position is either rotated or translated along the optical axis, the magnetic field also changes in orientation and strength, altering the magnitude and direction of the magnetic force experienced by the superparamagnetic bead. Bringing the magnet closer to the sample increases the tension on the tether, and the opposite is true as well. Rotating the magnet causes the superparamagnetic beads to rotate. The rotation of the superparamagnetic beads, in turn, exerts a torque on the DNA molecule, ultimately inducing it to supercoil. An overview of these interactions is depicted in Figure 11.

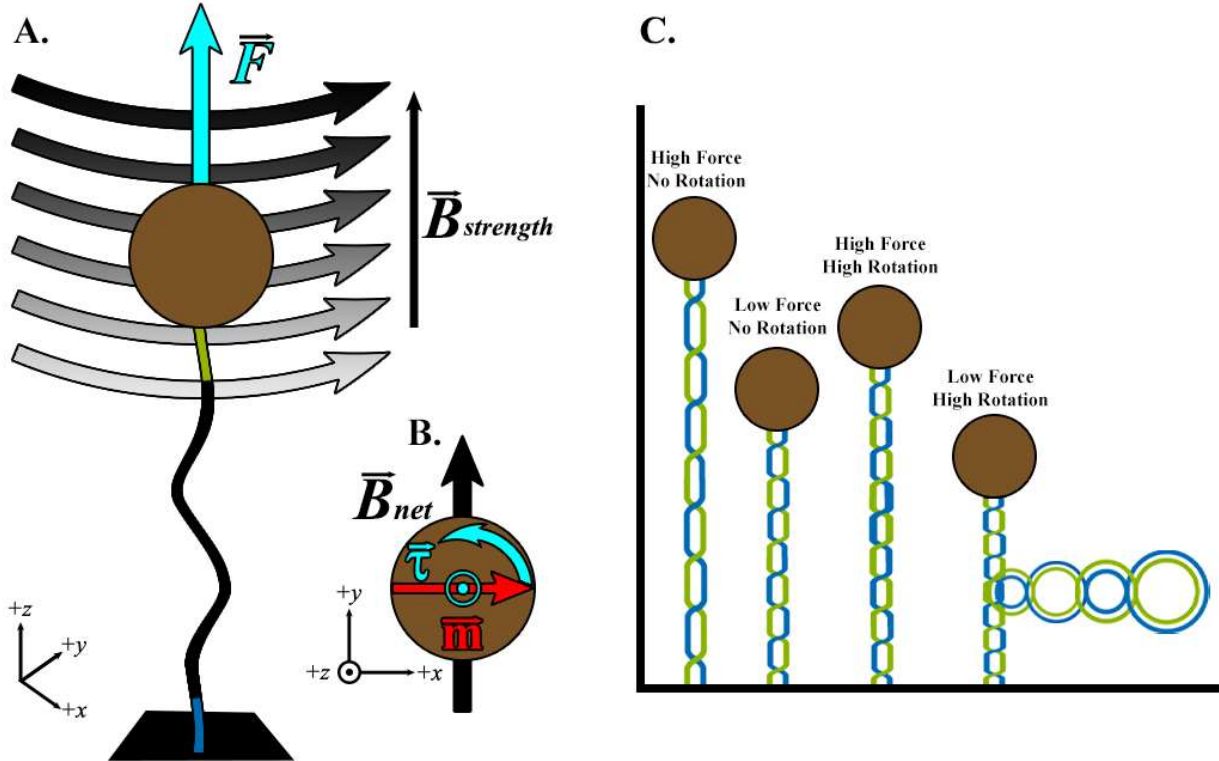


**Figure 11.** Diagram of  $B$  Induced Forces On Beads. **A.** Side view of a DNA (black line) tether bound to a superparamagnetic bead (brown) at one end (green) and to a surface (black quadrilateral) on the other end (blue). The tether is in the presence of the magnetic field  $B$  which decreases in magnitude. The bead's magnetic moment will align with the external magnetic field and an attractive force on the bead that translates to a pulling force  $F$  (cyan) will be exerted on the tether. **B.** To induce torque, the magnetic field is rotated, causing a misalignment of the bead's magnetic moment. Torque (cyan) is applied until the magnetic moments realign, so continuously rotating the field will induce turning, and therefore supercoiling of the DNA molecule attached to the bead. **C.** Different conformations of the same DNA are achievable by changing both the magnitude of the pulling force on the bead and the number of full rotations of the bead. Plectonemic supercoiling is shown in the figure at low force with a high number of rotations.

As stated previously, MT experiments facilitate the measurement of the extension DNA tethers and the calculation of the applied force, all in real time. The magnetic field has been shown to exert a stretching force  $F$  (N) on the tether:

$$F = \frac{1}{2} \nabla (m \cdot B) \tag{7}$$

where  $m$  ( $\text{A}\cdot\text{m}^2$ ) is the induced magnetic moment of the bead and  $B$  (T) is the magnetic field. A torque  $\tau$  ( $\text{N}\cdot\text{m}$ ) can also be induced through manipulation of the magnetic field parallel to the immobilization surface, given by:

$$\tau = m_0 \cdot B \quad (8)$$

where  $m_0$  is the minor component of the magnetic moment that is not initially aligned with the magnetic field  $B$ .<sup>9</sup> The application of torque to the DNA tether is able to induce supercoiling, altering the linking number of the molecule.

Live tracking of the position of the paramagnetic beads is achieved by observing samples under a magnetic tweezer microscope that was custom built (Figure 12) and analogous in design to those described elsewhere in literature.<sup>1,13,19,23,25-27,29</sup> The two permanent magnet MT microscopes in the Finzi lab consist of a Nikon Plan 100x/1.25 oil immersion objective (Nikon Instruments Inc. Melville, NY), a P-721 Piezo Flexure Objective Scanner (PI Physik Instrumente LP “PI” Auburn, MA), a tube lens  $f=160$  mm (Thorlabs Inc. Newton, NJ), two piezo motors (PI) for permanent magnet rotation and translation along the optical axis, and a Basler acA2000-165 $\mu\text{m}$  camera (IVS Imaging, Coppel, TX). A customized LED bright field illuminator (Luxeon Star LEDs, Quadica Developments Inc. Brantford, ON, Canada) is used to illuminate samples. Tweezing is achieved through vertical and rotational translations of two 1/2” x 1/4” x 1/8” N52-grade neodymium rare earth magnets mounted on a custom adjustable stage, separated by 1 mm.<sup>29</sup>

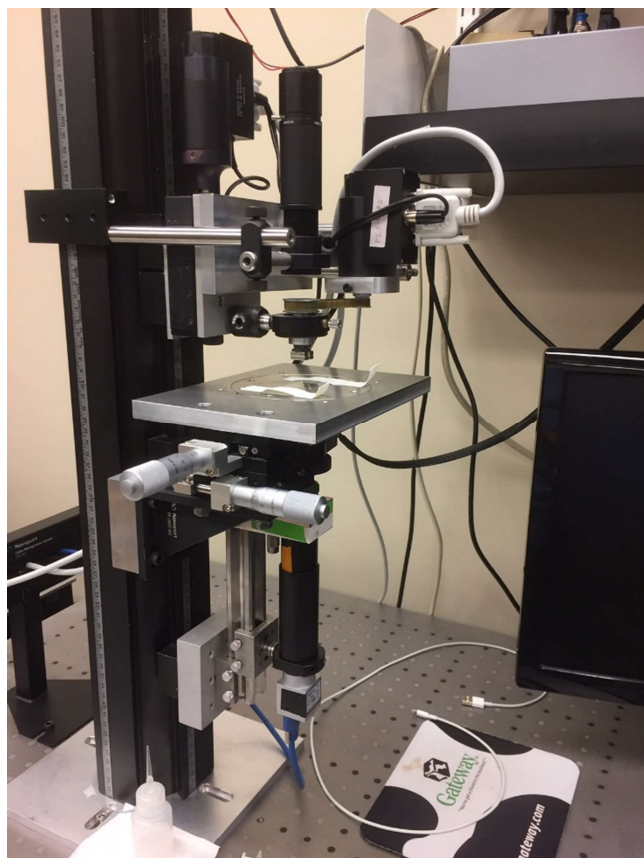


**Figure 12.** Magnetic Tweezer Microscope. This is one of the two microscopes in the Finzi Lab. Flow chambers with samples are placed on the stage and observed by the microscope from below. Two neodymium magnets are mounted above the stage and are used to generate the magnetic field that is used to manipulate samples.

As the wavelength of the red LED light ( $0.635 \mu\text{m}$ ) is similar in scale to the diameter of the superparamagnetic MyOne beads ( $1 \mu\text{m}$ ) (Invitrogen), circular diffraction patterns are generated around the center of the bead. These diffraction rings increase in diameter as the bead moves away from the focal plane.

Displacement in the  $z$  direction is calculated by best matching the radial profile of diffraction pattern intensity with specific intensity patterns in a lookup table, and displacement in the  $x$  and  $y$  directions is calculated using a radial symmetry detection algorithm based on real-time, 3D particle tracking.<sup>7,18,29</sup> The software incorporates a graphical user interface (GUI) which facilitates the recording of these data and allows the user to readily generate figures in MATLAB (MathWorks Natick, MA) with relative ease. The code for the microscope controls, 3D tracking, and force calculations software is all MATLAB (MathWorks) based, and Micromanager ([micro-manager.org](http://micro-manager.org)) is responsible for bridging the software with the MT microscope electrical hardware. All of the code is located here.<sup>34</sup>

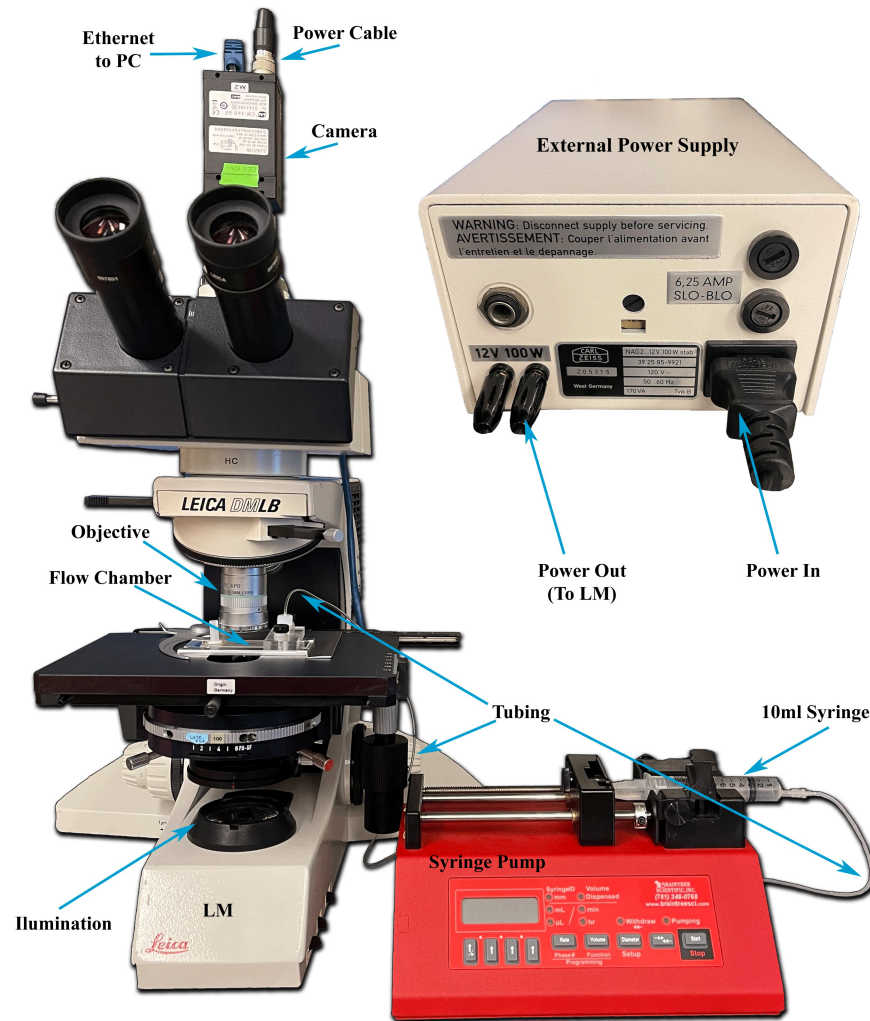


**Figure 13.** Leica Light Microscope (LM) and Pump System. This microscope was used for flow tests. The first set up for flow testing did not include the pump system or slide adapter, requiring flushes of the flow chamber to be performed using the micropipette-tissue strategy. Samples are loaded into flow chambers and placed on the stage. A camera transmits video feed to a program on the computer responsible for recording and storing videos (not shown).

### Flow Tests: Bulk Flow & Bead Displacement Tracking

To increase the area of the field of view (FOV) in which to visualize beads in fluid flow, we switched to using a 20X objective and a large pixel format camera, as the FOV from the 63X objective of the MT microscope covers too small an area for even proper visualization of moving particles. Briefly, samples were observed under a DMLB 100T light microscope (Leica Camera AG “Leica” Wetzlar, Germany) equipped with an HC PL APO 20x/0.70 mm oil immersion

objective (Leica), powered by an external 100W power supply (Carl Zeiss AG Jena, Germany) (Figure 13).

Video data is recorded by a CM-140 GE camera (JAI A/S Copenhagen, Denmark) and stored in an MP4 container format (H.264). Videos are recorded at a frame rate of approximately 30 frames per second (fps) using the *eBUS Player for JAI* software (Version 6.1.4.5137; Pleora Technologies Inc. Ottawa, Canada). This software does not have any tools that facilitate live particle tracking, or even displacement tracking as it only interfaces the camera with the computer for video recording purposes. For this reason, I wrote custom software to facilitate the collection of data regarding a bead's XY positions from the video recordings. These data, along with the respective times and frames of the videos at different positions along a bead's trajectory are manually recorded with the help of the program. These values are then used to calculate bead average velocities and taken as proxies for the bulk flow rate of the solution. The equation used to calculate average velocity from bead displacement (in pixels) is:

$$v = \frac{\sqrt{(x_2 - x_1)^2 + (y_2 - y_1)^2}}{\Delta t} \quad (9)$$

Average velocities are calculated twice, once using the difference in timepoints and once using the difference in frame count to calculate  $\Delta t$ . A screenshot of the program is provided in Figure 14, for reference.

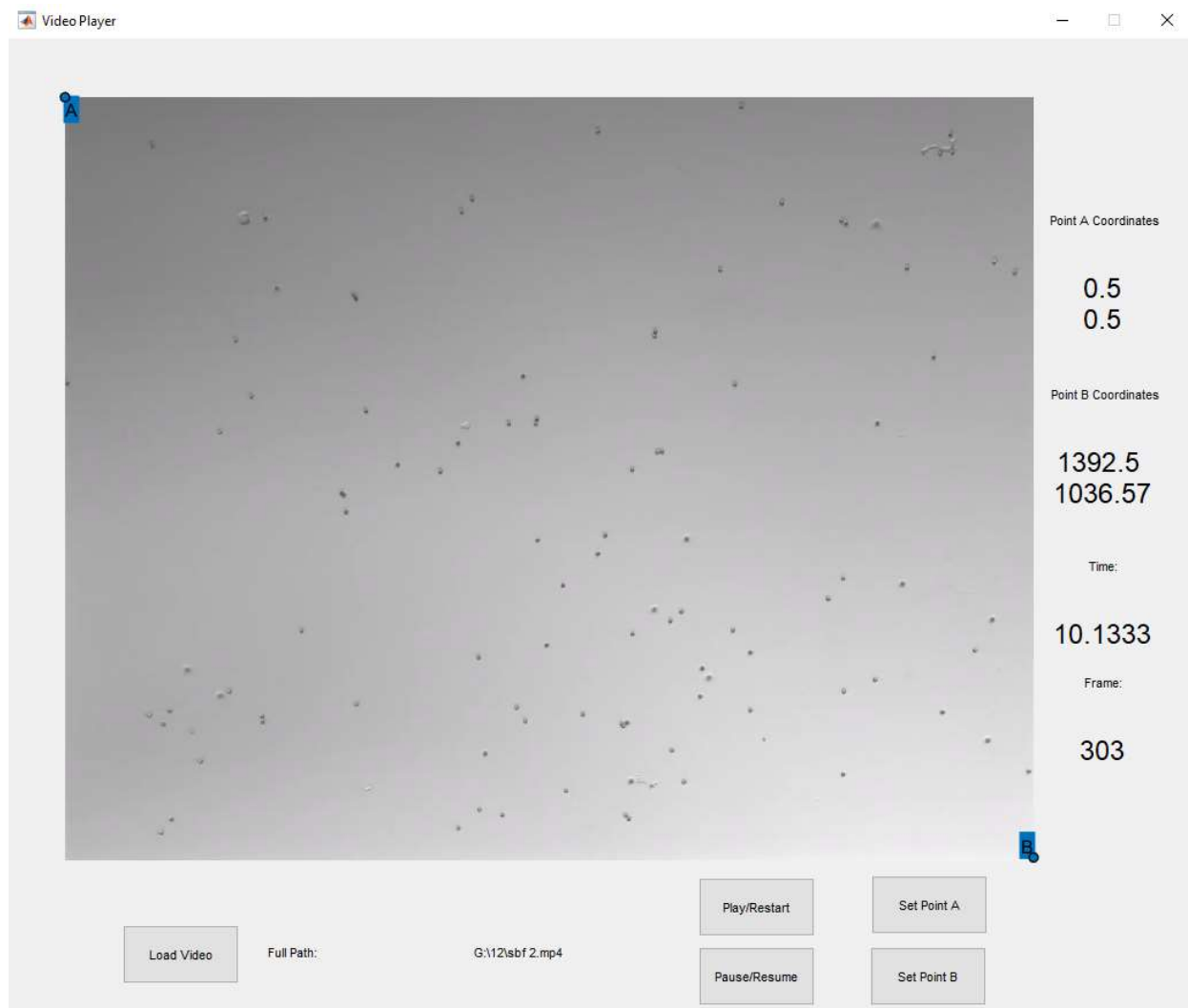


**Figure 14.** Custom Video Player GUI. This is a screenshot of the graphical user interface (GUI) of the video player developed to facilitate the calculation of bead velocities. The program incorporates buttons that allow the user to select a video file from their directory, play or restart the video, pause or resume the video, and select specific points on the video to display their coordinates in pixels. Velocity calculations must be performed manually using the values recorded with the video player, and pixel distances must be converted into physically meaningful distances using a conversion factor.

## **Chapter III: Results**

### Magnetic Tweezer Tests

During a MT experiment, bead displacement in the  $x$ ,  $y$ , and  $z$  directions as well as the distance of the magnet from the glass surface of the flow chamber is measured as a function of the total number of turns the magnets and the direction of those turns. By adjusting the height and rotation of the magnets, tension and torque forces can be exerted on tethers to induce conformational changes in dsDNA, as depicted by Figure 11C in Chapter 2.

If the strength of the magnetic field generated by the permanent magnets decreases as the distance to the magnet increases, then it follows that as the magnets are brought closer to the sample, the forces exerted by the field on the tether will increase. This is supported by the *Force vs Magnet Height* curve (Figure 15A). Furthermore, the effective length of the tether is shown to be dependent on the relative height of the magnet from the sample, with greater tether lengths measured at shorter distances between the sample and the magnets. Figure 15B shows the dependence of the tether length on magnet height and finally Figure 15C shows the dependence of the DNA extension on the force, although conventionally this is plotted as *Force vs. Length*. The two plots consistently show that DNA end-to-end distance increases as the magnets are moved closer to the sample tension increases. To determine the end-to-end distance of a tether (tether extension), one calculates the difference between the coordinates of a tethered bead and a stuck bead. Figure 15D is an image of the FOV of MT microscope, showing what is displayed on-screen during operation of the MT microscope.

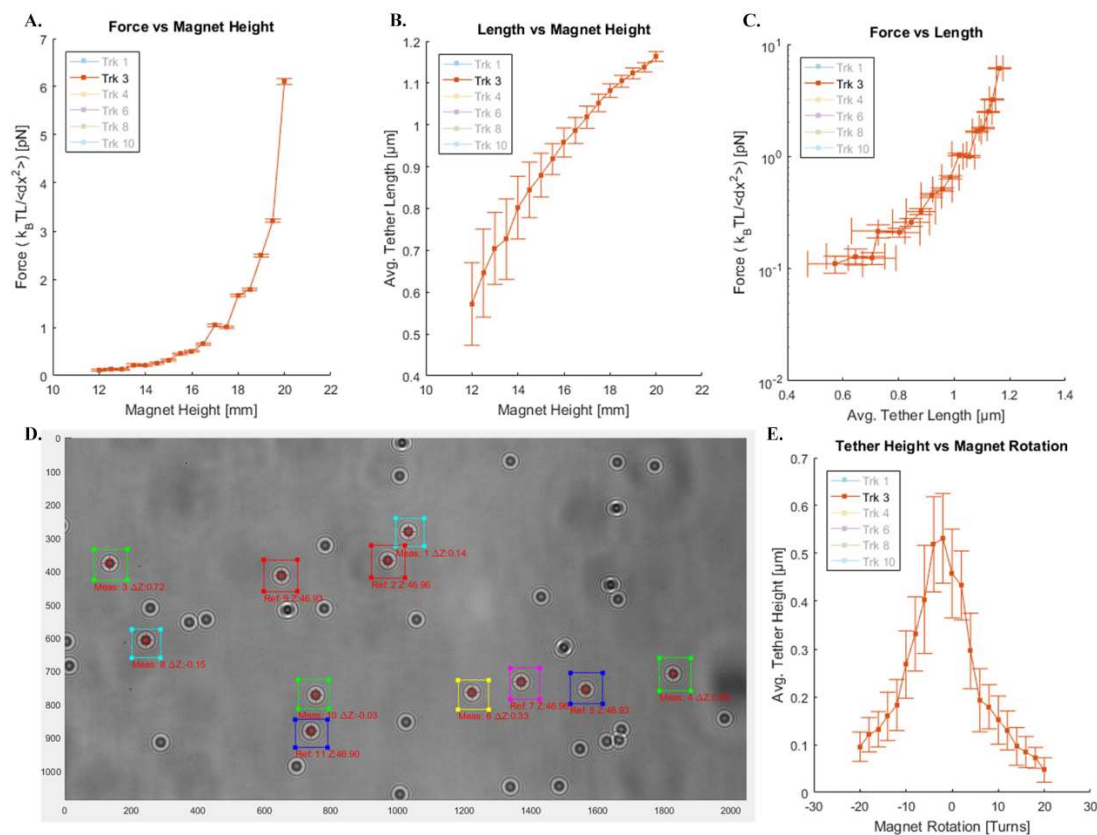


**Figure 15.** Magnetic Tweezing Experiments and Sample Field of View. **A.** Force calculation curve based on the data collected from the previous manipulation experiment showing that the force exerted on the tether increases as the distance of the magnets to the glass coverslip decreases. **B.** Data recorded from a manipulation experiment measuring the change in average tether length due to a change magnet distance from the sample. As the distance between the magnets and the sample decreases, the average tether length increases. **C.** A force calculation curve based on the previous manipulation experiment showing that the average length of the tether increases as the force exerted on the tether increases. **D.** A model FOV of the magnetic tweezer microscope. This is what the operator sees while observing a sample and tracking beads. **E.** Data recorded from a manipulation experiment that involves rotating the magnets to exert a torque on the DNA tether and induce supercoiling. The average tether length decreases as the amount of supercoiling of the DNA increases, and the opposite is true also.

It was previously stated that inducing torque on beads attached to a dsDNA tether and causing them to rotate would cause a change in the linking number of the nucleic acid and inducing supercoiling. Intuitively, one would imagine that as the number of full rotations of the magnet increases that the supercoiling intensity would also increase. The plot showing the tether height

in relation to the number of 360° turns of the magnets shows that the height of the tether decreases as the number of full magnet rotations increases (Figure 15E). Noticeably, the curve is symmetric between -20 and 20 turns, recorded at a magnet height of 12 mm. This is consistent with the theoretical model shown in Figure 11C. These results demonstrate that the generated DNA tethers produced following the protocol detailed in Chapter 2 are coilable and suitable for further experimentation. Despite this success, it soon became apparent that reproducibility of the measurements was not satisfactory. In particular, the density of tethers in any given field of view was never constant within the same chamber and among different chambers. I also realized that this was a problem encountered by other members in the lab. Therefore, I set out to work on a protocol to address this variability.

#### Flow Tests using Tissues and Micropipettes

The objective of measuring the displacement of beads over periods of time to calculate their average velocities is to provide a more accurate understanding of the interactions and conditions generated during flow chamber preparation and sample loading and buffer exchange.

Consequently, the intended purpose of flow testing (FT) is to facilitate the standardization of the protocols used by the Finzi Lab when preparing samples for, and conducting, single molecule experiments. The hope is that standardizing practices in microchamber preparation and design, as well as sample preparation and loading techniques will allow us to consistently obtain supercoilable tethers at substantial tethering densities and facilitate further single molecule experimentation.<sup>12,15</sup> Observation of the bulk flow of buffer solution, DNA tethers, and unbound beads was achieved by the use of light microscopy in the absence of a magnetic field, generating conditions similar to those during sample preparation and loading in the microscope flow chamber.

The protocols used to prepare samples for flow chambers used in both TPM and MT experiments in our lab rely on the use of capillary action to introduce buffer across microchambers, which is performed manually. Both sample loading and flushing has to be performed using a micropipette held steadily at the flow chamber inlet, and a Kimtech tissue wipe (Kimberly-Clark Corporation Irving, Texas) twisted into a tip held at the outlet of the flow chamber (Figure 16). While pipetting solution into the entrance well, tissue paper is pressed against the exit well, drawing liquid through the flow chamber and into the tissue via capillary action. Based on simple practical observation as well as FT, it became evident that solution flow speeds are affected by a wide range of factors including the dampness of the tissue, the shape and compactness of the twisted tissue tip, and the volume of tissue contacting the buffer in the exit well of the flow chamber. Clearly there are a number of limitations associated with this approach, and the speed of buffer flow across different samples is virtually impossible to reproduce, thus the variability in sample preparations.

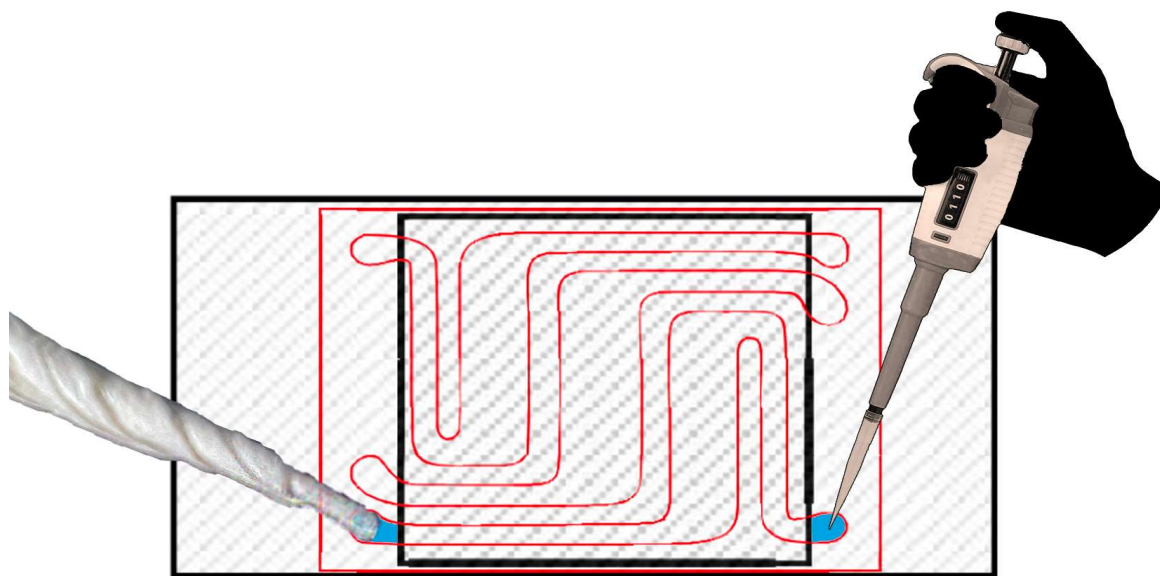


**Figure 16.** Micropipette-Tissue Sample Loading Strategy. Using a micropipette, solution (blue) is deposited at the inlet while simultaneously withdrawing solution from the outlet. The wells of the parafilm gasket (red) are left exposed by the glass (black).

Initial FT performed using the method of micropipette and twisted tissue very quickly demonstrated that solution flow rates, as visualized by bead velocities, were highly variable even between different flushes of the same sample. The average *measured* bead velocities can range from anywhere between 50 to over 500  $\mu\text{m/s}$  between flushes, and even within a single flush, moving extremely quickly over very short periods of time. Velocities were calculated manually using the distance values obtained using the video player software. The acceleration of the beads is often so rapid that it appears as though beads instantaneously transition from floating idly to moving at immeasurable speeds across the FOV. At velocities greater than 500  $\mu\text{m/s}$  it becomes difficult to track beads because they become increasingly blurred as the camera shutter speed is not rapid enough. Warping of the perceived shape of the bead from circular to elliptical, and even nearly linear, makes velocity calculations virtually impossible, as well as inaccurate. Not surprisingly, when adopting the tissue-micropipette strategy for sample loading and flushing, bead velocities are immeasurable more often than they are measurable, simply due to the operator's inability to replicate both tissue construction and positioning between flushes.

#### Flow Tests with Pump Implementation

The clear lack of consistency even within a single flush of the flow chamber when using the tissue-micropipette strategy indicates that an improved, more reproducible approach to sample loading is necessary. This need is compounded by the fact that obtaining clear videos at a stable distance from the objective proves to be excruciatingly difficult, given that minimal drift moves the tethers out of the focal point of the lens. For this reason, a fluid pump system was implemented to assist with buffer loading and washing steps, as we hypothesized it would decrease the variability in flow rates, increasing sample preparation efficiency, preventing damaging influences from uncontrolled forces, and increasing reproducibility across trials.

The pump system solution utilizes a programmable BS-8000 syringe pump (Braintree Scientific, Inc. Braintree, Massachusetts) which operates a 100 ml syringe (Becton, Dickinson and Company Franklin Lakes, New Jersey) attached to watertight flexible tubing that can be used to withdraw solution from the exit well of a flow chamber. A picture of the pump system was included in Figure 13. The tubing connects to a tapered 1/16" flangeless fitting connector and ferrule, which screw into a custom-built plexiglass manifold. This manifold, in turn, screws into a custom-built aluminum frame designed to support a 3" x 1" glass microscope slide. See figure 17 for chamber adapter design. Both the aluminum frame and the plexiglass manifold were designed and assembled by Dr. Dunlap (Figure 17A).

There are a few differences between previous flow chamber designs and the flow chamber design used in conjunction with the pump system. A larger top coverslip is used so that it leaves only the entrance well completely exposed, while at the same time extending past the exit well, a feature exclusive to this chamber design (Figures 17 B and C). The well is exposed through an opening in the coverslip made by the same laser cutter used to cut gaskets. Moreover, the entrance well of the flow chamber is not left exposed but is instead encompassed by a ferrule that serves as both a buffer reservoir and as a barrier between the entrance well and its immediate vicinity. All connections, such as the one between the exit hole in the top coverslip and the tubing, need to be water-tight, so small parafilm squares with holes etched in the middle were cut using the laser cutter in order to seal the connections where leakage is likely to occur.

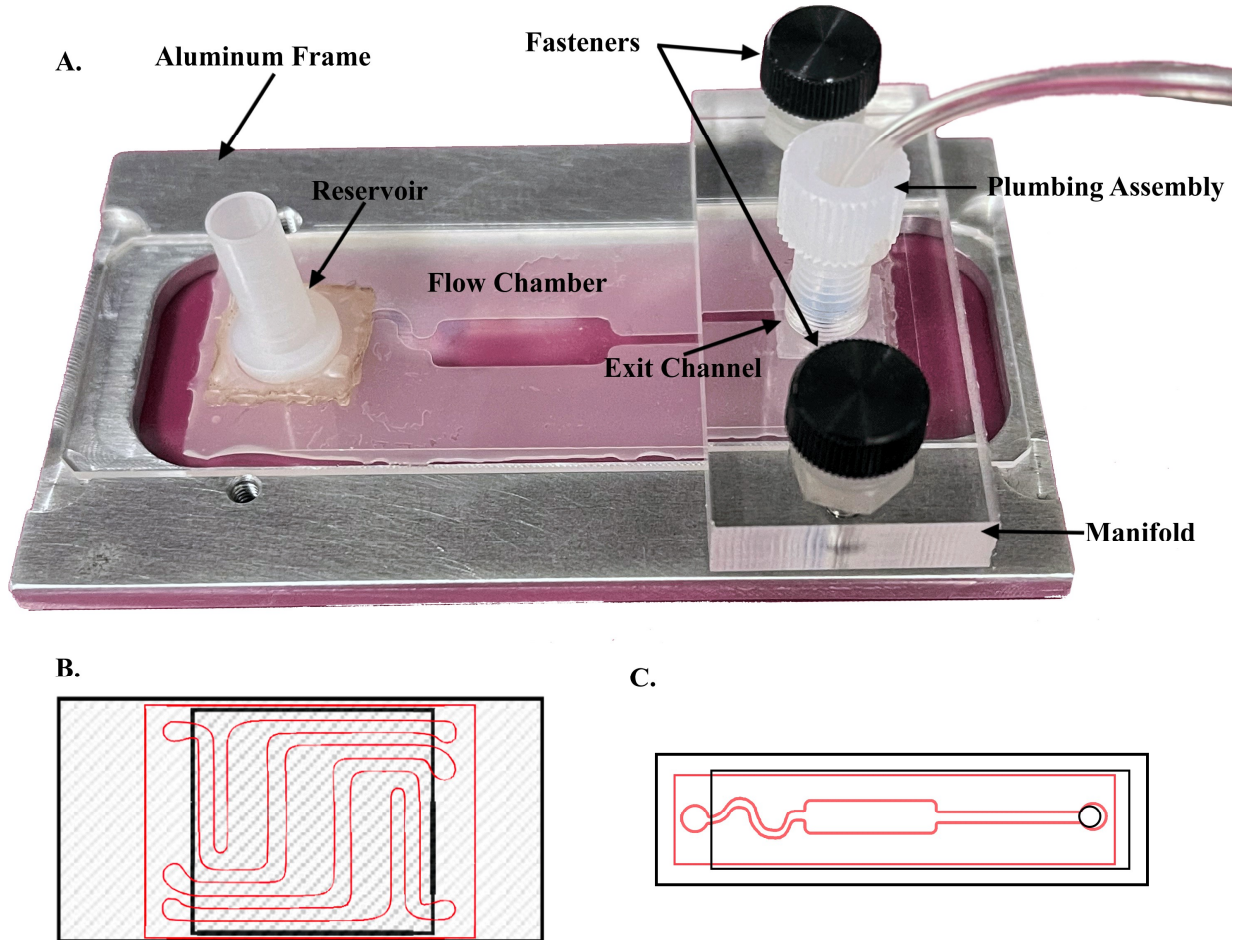


**Figure 17.** Flow Chamber and Slide Adapter Design. **A.** Labeled picture of the slide adapter used to house flow chambers and incorporate the fluid pump system. **B.** A diagram of the previous flow chamber design based on sandwiching a parafilm gasket between 24x50 and 22x22 mm coverslips, leaving all entrance and exit wells exposed. **C.** A diagram of the current flow chamber design sandwiching a parafilm gasket between a 3" glass microscope slide and a 24x50 mm coverslip. The entrance well is left completely exposed, while the coverslip extends past the gasket with only the drilled hole exposing a large portion of the exit well

Collected video data provides evidence that the rate of the bulk flow of the solution is much more stable and adjustable when the pump system is implemented for FT. The ability to set the rate of fluid withdrawal at a specific value on the pump largely eliminates the variability within any given flush, as measured by the velocities of the beads. The settings on the pump provide a

mechanism to control the flow, which has to be calibrated for every setting on the pump to know the actual flow rates of solution in the chambers. With the pump system it is possible to limit flow rates to roughly  $50 \mu\text{m/s}$ , while withdrawing fluid at rates between  $250\text{-}300 \mu\text{l/hr}$  on the pump, given the current flow chamber design. Bead average velocities and the variance between them decreased dramatically once the pump was implemented (Figure 18). The pump system maintains a constant withdrawal rate throughout an entire flush, something that is impossible to achieve using manual loading techniques. The frequency of beads traveling at immeasurable velocities is significantly reduced as well. Finally, collection of video data for the duration of entire flushing steps also provided the opportunity to make both qualitative observations of the flushing process and its effects within the confines of the flow chamber and quantitative measurements of the flow rates of beads.

Due to the preliminary state of the pump arrangement design and the differences in total volume of each flow chamber, bead velocities are not identical between flow chambers even when the withdrawal settings on the pump are maintained. Flow chamber gaskets of different dimensions have different internal volumes, leading to different fluid velocities at identical pump settings.

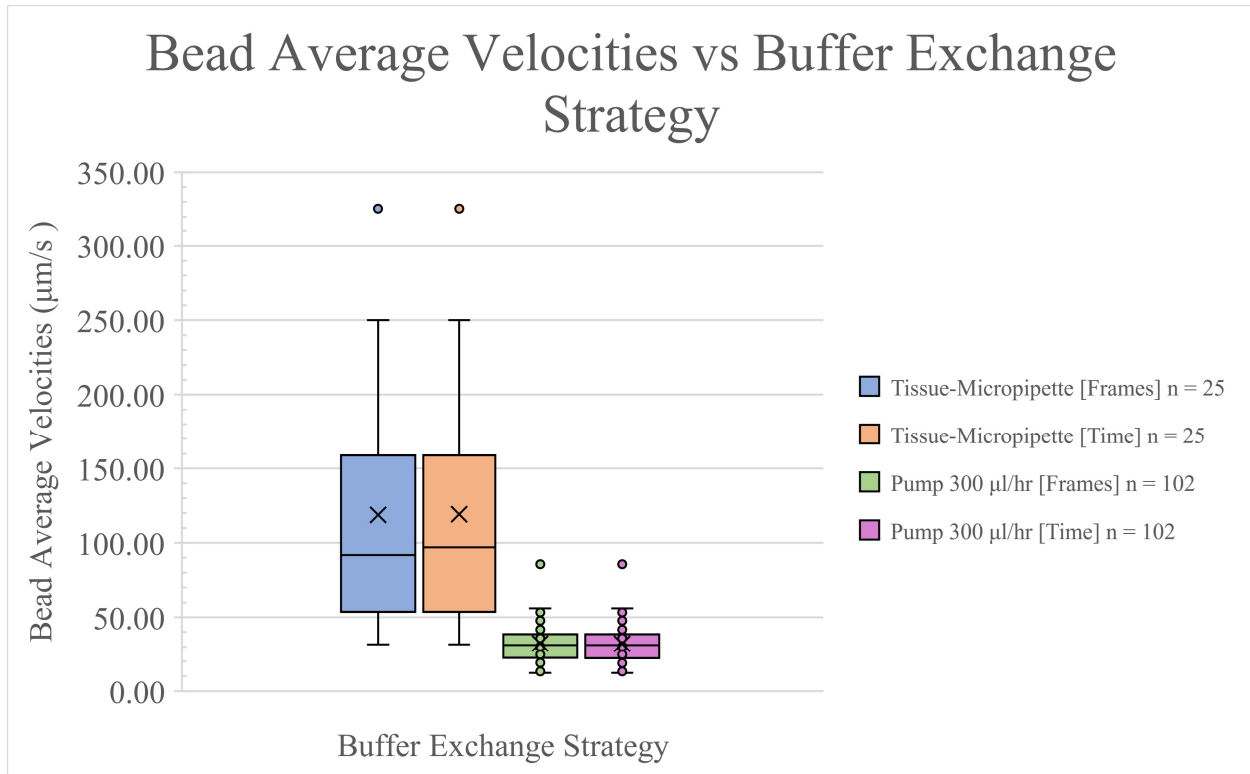


**Figure 18.** Bead Average Velocities vs Buffer Exchange Strategy. The chart shows that there is a substantial difference in variability in measured bead average velocities between buffer exchange approaches. The variability of the flow rates decreases significantly once the pump is implemented. The average and median average velocities are also substantially lower for the pump withdrawal strategy. The two box plots on the left represent measurements obtained using frames (blue) or timepoints (orange) to calculate bead average velocity using the Tissue-Micropipette strategy. The two box plots on the right represent measurements obtained using frames (green) or timepoints (purple) to calculate bead average velocity withdrawing solution at 300 μl/hr with the pump system.

## **Chapter IV: Discussion**

### Making A New DNA Tether for MT Measurements of Protein-Constrained Torsion

In the first part of my work, I successfully prepared a DNA tether that could be anchored through multiple digoxigenin links to the glass surface of a MT microscope flow chamber at one end, and through multiple biotin links to a 1 micron, streptavidin-coated paramagnetic bead at the other end. This tether contained three nicking sites for quick relaxation of torsion deriving from twisting the molecule with MT in control measurements and from proteins in the experiments of interest. The hope was to make use of the nicking sites by introducing a nicking enzyme to quickly release the torsional constraint on the molecule under turns of the magnets. Despite the success in preparing the tethers, the variability in the MT microchamber sample preparation led me to tackle this problem for the remainder of my thesis project.

### Implementation of a Pump Flow System for Reproducible Chamber Preparations

We identified the non-reproducible flow rates that derived from using a Kimwipe manually positioned to wick fluid from the outlet of the chamber as the main source of variability in the yield of tethers in different chambers. Exposure of experimental samples to uncontrolled and extremely variable velocities can be damaging to the tethers, as demonstrated, for example, by the disappearance of a tethered bead from the FOV in the middle of particle tracking. In an attempt to reduce, if not eliminate, such variability, we implemented the use of a pump and I tested its effect on the flow rate of both DNA tethers and free beads in solution. Using tissues to draw solutions into the chamber resulted in average velocities of beads often much greater than 500  $\mu\text{m/s}$ , being immeasurable with the available instrumentation, suggesting that the magnitude of the forces exerted by the bulk flow of the solution can often be very substantial. Furthermore,

measurements recorded using the video player software I developed demonstrated a very significant decrease in both variability and average bead velocities when the pump is used to withdraw solution.

Video data collected from the FT demonstrates that even after attempts are made to provide reproducible flow rates, other factors remain that would be helpful to address. For example, all recorded videos of flow tests, both employing the pump system and without it, contained footage of debris being ushered along by the flow of the solution. Gasket debris is relatively small and usually only travels around the perimeter of the chamber, near the parafilm walls. On the other hand, much larger debris (a few hundred times larger than any bead) can be seen traversing the flow chamber more often towards the center. The effects of this kind of debris are more concerning than that of gasket debris, as they can often be seen bouncing off the glass surfaces and knocking into tethers, dislodging them from their points of attachment on the functionalized microscope slide. Even at slower flow rates ( $<100 \mu\text{m/s}$ ), the larger debris will still dislodge a significant proportion of the tethers it comes into contact with, so it should come as no surprise that increasing velocity will increase the number of affected tethers. It is very unlikely that debris in samples can be totally eliminated, but extreme care should be used when preparing all reagents and buffer components. Steps that include washing the parafilm gaskets after cutting and storing them in dry and sterile environments will limit the number of debris generated by the gasket itself. The attachment of a ferrule around the entrance well eliminates contact between micropipette tip and the cleaned glass while also forming a relatively tall physical barrier between the entrance to the chamber and its immediate surroundings. This should also help keep contaminants out of the flow chamber.

Another major limitation that this experiment faced was the lack of any commercially or publicly available tool to analyze bead tracking data that is stored in .MP4 video formats. Conceptually, measuring the velocity of the flow of beads in a sample is a relatively straightforward: the bead's total displacement of a bead within a given period of time, as well as its direction and divide the component in the flow direction by the time. In practice however, this is hardly the case.

Measurements must be made from captured videos, which presents a totally new set of challenges than making measurements. Videos are displayed in pixels, therefore bead positions recorded from videos must be converted to physically representative values using a conversion factor; a calibration slide was used for this purpose. Furthermore, the corresponding frame at each measured positional coordinate must be recorded because of its use in velocity calculations. To overcome these challenges, a digital tool to facilitate the collection of data from the videos recorded with the camera software was required. This tool, needed to allow the user to select and import video files, play, pause, and restart the videos, select multiple points on the video and display their coordinates (in pixels), and display the current time and video frame. My solution was to create a multifunctional video player that can be used to record the desired information. The program was coded in MATLAB (MathWorks), for compatibility with the other custom developed software in the Finzi lab. The full code for the program is included in Appendix B.

Since the program is small and does not require tremendous amounts of computing power, data analysis can be performed on virtually any computer that can run MATLAB (MathWorks) and is likely to be useful for other single molecule experiments that require analysis of raw video footage. This contrasts with the MT software, which is specific to the custom microscopes and data formats. The open-source nature of the software will facilitate updating the program developed for the flow testing experiments and incorporating new features. A key feature that I

am looking to incorporate for future experimentation is the automated tracking of beads using a computational algorithm. One option that appears promising would be the integration of a Kalman filter to identify particle positions for displacement measurements.<sup>33</sup>

### Future Objectives and Outlook

Given that both particle tracking and virtually all calculations for MT tests are performed using automated algorithms by the computer, it should be apparent that any disturbances in bead motion not due to thermal Brownian diffusion or the induced magnetic field will generate errors during calculations. I observed that fibers and other debris in the fluid can collide with tethers and remove them completely, compromising any experiments being conducted on the tether.

When considered along with the fact that the micropipette-tissue strategy generates irreproducible loading conditions and highly variable fluid flow rates, it is clear that the sample loading protocol and any subsequent chamber flushing should ideally be performed using a pump system, such as the one detailed here.

Control of the fluid flow rates is especially important for single molecule experiments in which buffer exchange occurs in the flow chamber between data collection steps.<sup>12,15</sup> In the near future, the Finzi lab aims to use magnetic tweezer manipulation to monitor the changes in compaction of supercoiled DNA as nucleoid-associated proteins<sup>4</sup> dissociate from the tether due to increased tension. The proposed experimental strategy involves preparing DNA tethers, inducing various degrees of supercoiling using the MT, introducing DNA-binding proteins into the system, relaxing the torsional strain on the tether, and finally applying high tension to trigger dissociation of attached proteins. The hypothesis is that dissociation will produce discrete increases of tether extension, which can be counted to determine the number of proteins previously bound to the tether. Clearly, this experiment and others like it require multiple exchanges of solution.

Therefore, well-controlled rates of fluid flow during sample loading and buffer exchange will greatly improve the experimental throughput and increase reproducibility across samples.

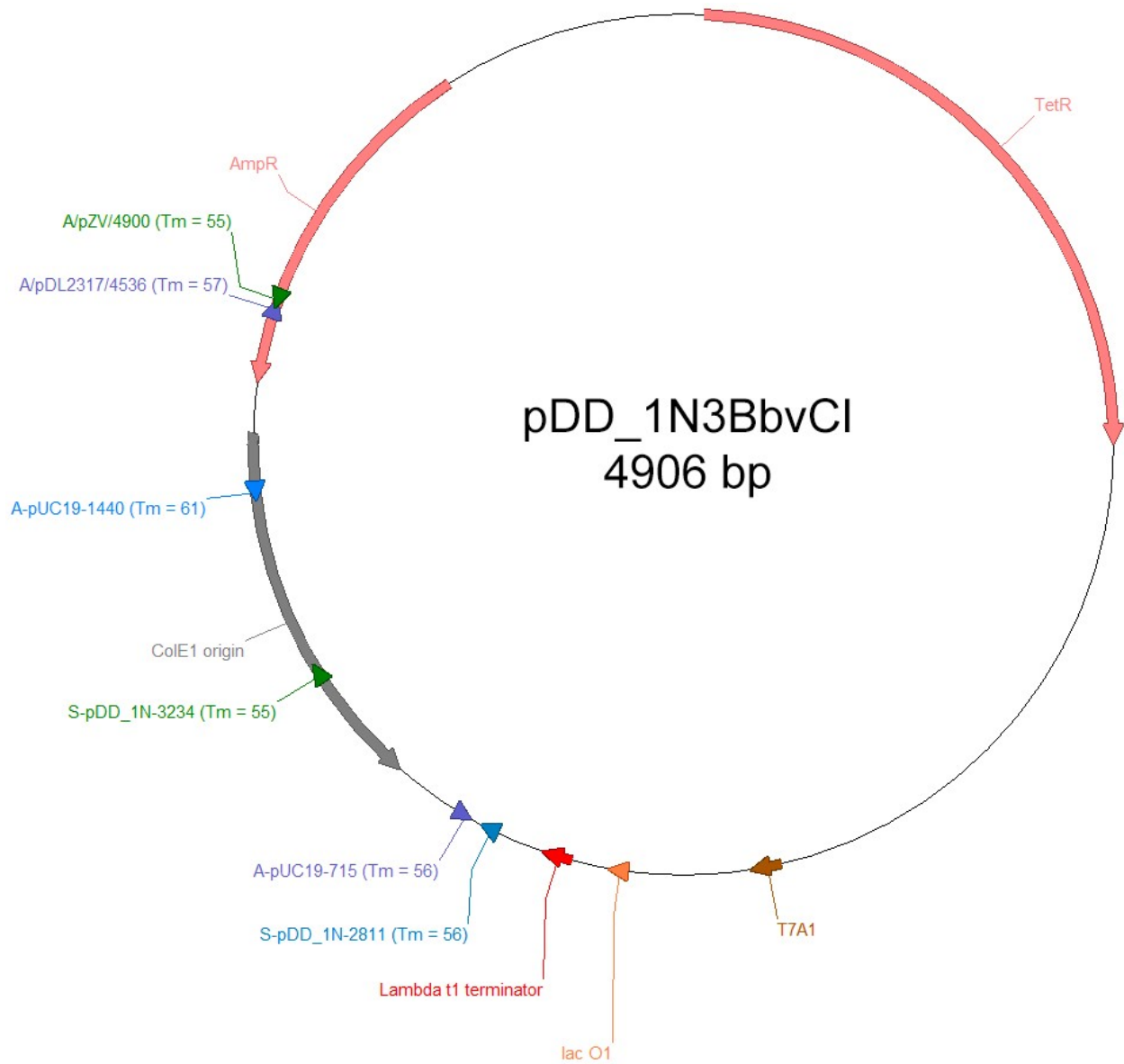
### References:

1. Abels, J.A., Moreno-Herrero, F., van der Heijden, T., Dekker, C., Dekker, N.H., 2005. Single-Molecule Measurements of the Persistence Length of Double-Stranded RNA. *Biophysical Journal* 88, 2737–2744. <https://doi.org/10.1529/biophysj.104.052811>
2. Belkebir, A., Azeddoug, H., 2013. Metal ion dependence of DNA cleavage by SepMI and EhoI restriction endonucleases. *Microbiological Research* 168, 99–105. <https://doi.org/10.1016/j.micres.2012.08.003>
3. Crick, F., 1970. Central Dogma of Molecular Biology 3.
4. Cristofalo, M., Marrano, C.A., Salerno, D., Corti, R., Cassina, V., Mammola, A., Gherardi, M., Sclavi, B., Cosentino Lagomarsino, M., Mantegazza, F., 2020. Cooperative effects on the compaction of DNA fragments by the nucleoid protein H-NS and the crowding agent PEG probed by Magnetic Tweezers. *Biochimica et Biophysica Acta (BBA) - General Subjects* 1864, 129725. <https://doi.org/10.1016/j.bbagen.2020.129725>
5. Dawkins, R., 2006. *The selfish gene*, 30th anniversary ed. ed. Oxford University Press, Oxford ; New York.
6. Finzi, L., Dunlap, D.D., 2010. Single-molecule Approaches to Probe the Structure, Kinetics, and Thermodynamics of Nucleoprotein Complexes That Regulate Transcription. *Journal of Biological Chemistry* 285, 18973–18978. <https://doi.org/10.1074/jbc.R109.062612>
7. Gosse, C., Croquette, V., 2002. Magnetic Tweezers: Micromanipulation and Force Measurement at the Molecular Level. *Biophysical Journal* 82, 3314–3329. [https://doi.org/10.1016/S0006-3495\(02\)75672-5](https://doi.org/10.1016/S0006-3495(02)75672-5)
8. Gruber, S., Löf, A., Sedlak, S.M., Benoit, M., Gaub, H.E., Lipfert, J., 2020. Designed Anchoring Geometries Determine Lifetimes of Biotin-Streptavidin Bonds under Constant Load and Enable Ultra-Stable Coupling (preprint). *Biophysics*. <https://doi.org/10.1101/2020.05.12.090639>
9. Kessler, C., Mantas, V., n.d. Specificity of restriction endonucleases and DNA modification methyltransferases - a review (Edition 3) 240.
10. Lehninger, A.L., Nelson, D.L., Cox, M.M., 2013. *Lehninger principles of biochemistry*, 6th ed. ed. W.H. Freeman, New York.
11. Lewis, M., Chang, G., Horton, N.C., Kercher, M.A., Pace, H.C., Schumacher, M.A., Brennan, R.G., Lu, P., 1996. Crystal Structure of the Lactose Operon Repressor and Its Complexes with DNA and Inducer. *Science* 271, 1247–1254. <https://doi.org/10.1126/science.271.5253.1247>

12. Liebesny, P., Goyal, S., Dunlap, D., Family, F., Finzi, L., 2010. Determination of the number of proteins bound non-specifically to DNA. *J. Phys.: Condens. Matter* 22, 414104.  
<https://doi.org/10.1088/0953-8984/22/41/414104>
13. Lipfert, J., Hao, X., Dekker, N.H., 2009. Quantitative Modeling and Optimization of Magnetic Tweezers. *Biophysical Journal* 96, 5040–5049. <https://doi.org/10.1016/j.bpj.2009.03.055>
14. Madhus, I.H., 1988. Regulation of intracellular pH in eukaryotic cells. *Biochemical Journal* 250, 1–8. <https://doi.org/10.1042/bj2500001>
15. Marko, J.F., Xiao, B., Zhang, H., Johnson, R.C., 2011. Force-driven unbinding of proteins HU and Fis from DNA quantified using a thermodynamic Maxwell relation. *Nucleic Acids Research* 39, 5568–5577. <https://doi.org/10.1093/nar/gkr141>
16. Neuman, K.C., Lionnet, T., Allemand, J.-F., 2007. Single-Molecule Micromanipulation Techniques. *Annu. Rev. Mater. Res.* 37, 33–67. <https://doi.org/10.1146/annurev.matsci.37.052506.084336>
17. Pan, H., Xia, Y., Qin, M., Cao, Y., Wang, W., 2015. A simple procedure to improve the surface passivation for single molecule fluorescence studies. *Phys. Biol.* 12, 045006.  
<https://doi.org/10.1088/1478-3975/12/4/045006>
18. Parthasarathy, R., 2012. Rapid, accurate particle tracking by calculation of radial symmetry centers. *Nat Methods* 9, 724–726. <https://doi.org/10.1038/nmeth.2071>
19. Ribeck, N., Saleh, O.A., 2008. Multiplexed single-molecule measurements with magnetic tweezers. *Rev. Sci. Instrum.* 79, 094301. <https://doi.org/10.1063/1.2981687>
20. Schochetman, G., Ou, C.-Y., 2021. *Polymerase Chain Reaction* 5.
21. Sedlak, S.M., Schendel, L.C., Gaub, H.E., Bernardi, R.C., 2020. Streptavidin/biotin: Tethering geometry defines unbinding mechanics. *Sci. Adv.* 6, eaay5999.  
<https://doi.org/10.1126/sciadv.aay5999>
22. Sedlak, S.M., Schendel, L.C., Melo, M.C.R., Pippig, D.A., Luthey-Schulten, Z., Gaub, H.E., Bernardi, R.C., 2019. Direction Matters: Monovalent Streptavidin/Biotin Complex under Load. *Nano Lett.* 19, 3415–3421. <https://doi.org/10.1021/acs.nanolett.8b04045>
23. Seol, Y., Neuman, K.C., 2011. Magnetic Tweezers for Single-Molecule Manipulation, in: Peterman, E.J.G., Wuite, G.J.L. (Eds.), *Single Molecule Analysis, Methods in Molecular Biology*. Humana Press, Totowa, NJ, pp. 265–293. [https://doi.org/10.1007/978-1-61779-282-3\\_15](https://doi.org/10.1007/978-1-61779-282-3_15)
24. Slonczewski, J., Foster, J.W., 2016. *Microbiology: an evolving science*, Fourth edition. ed. W. W. Norton & Company, New York.
25. Smith, S., Finzi, L., Bustamante, C., 1992. Direct mechanical measurements of the elasticity of single DNA molecules by using magnetic beads. *Science* 258, 1122–1126.  
<https://doi.org/10.1126/science.1439819>

26. Strick, T.R., Allemand, J.-F., Bensimon, D., Croquette, V., 1998. Behavior of Supercoiled DNA. *Biophysical Journal* 74, 2016–2028. [https://doi.org/10.1016/S0006-3495\(98\)77908-1](https://doi.org/10.1016/S0006-3495(98)77908-1)
27. Vilfan, I.D., Lipfert, J., Koster, D.A., Lemay, S.G., Dekker, N.H., 2009. Magnetic Tweezers for Single-Molecule Experiments, in: Hinterdorfer, P., Oijen, A. (Eds.), *Handbook of Single-Molecule Biophysics*. Springer US, New York, NY, pp. 371–395. [https://doi.org/10.1007/978-0-387-76497-9\\_13](https://doi.org/10.1007/978-0-387-76497-9_13)
28. Vologodskii, A., 2015. *Biophysics of DNA*. Cambridge University Press, Cambridge. <https://doi.org/10.1017/CBO9781139542371>
29. Vörös, Z., Yan, Y., Kovari, D.T., Finzi, L., Dunlap, D., 2017. Proteins mediating DNA loops effectively block transcription: LacI-Mediated DNA Loops Are Strong RNAP Roadblocks. *Protein Science* 26, 1427–1438. <https://doi.org/10.1002/pro.3156>
30. White, J.H., 1969. Self-Linking and the Gauss Integral in Higher Dimensions. *American Journal of Mathematics* 91, 693. <https://doi.org/10.2307/2373348>
31. Xu, W., Finzi, L., Dunlap, D., 2020. Tethered Particle Microscopy, in: Roberts, G., Watts, A. (Eds.), *Encyclopedia of Biophysics*. Springer Berlin Heidelberg, Berlin, Heidelberg, pp. 1–4. [https://doi.org/10.1007/978-3-642-35943-9\\_489-1](https://doi.org/10.1007/978-3-642-35943-9_489-1)
32. Zampieri, S., Ghirardello, A., Doria, A., Tonello, M., Bendo, R., Rossini, K., Gambari, P.F., 2000. The use of Tween 20 in immunoblotting assays for the detection of autoantibodies in connective tissue diseases. *Journal of Immunological Methods* 239, 1–11. [https://doi.org/10.1016/S0022-1759\(00\)00168-X](https://doi.org/10.1016/S0022-1759(00)00168-X)
33. <https://www.mathworks.com/help/vision/ug/using-kalman-filter-for-object-tracking.html>
34. <http://www.physics.emory.edu/faculty/finzi/research/code.shtml>

Appendix A:



Sequence:

tatcacagttaaattgctaacgcagtcaggcaccgtgtatgaaatctaacaatgcgctcatcgtcatcctcggcaccgtcacctggatgctgtaggcataggcttggttatg  
 ccggtactgccgggctcttgcgggatatgctcattccgacagcatcggcagtcactatggcgtgctgctagcgtatagcgttggatgcaatttctatgcgacccgttct  
 cggagcactgtccgaccgttggccgccagctcctgctcgcctcgtacttggagcactatcgactacgcgatcggcgaccacaccgctcctgtggtatcctta  
 cgcgggacgcacgtggccggcatcaccggcgccacaggtgcggttgcggcctatcgcggacatcaccgatggggaagatcgggctgccactcgggctca  
 tgagcgttggcgtgggtatggggcaggccccgtggccggggactgtgggcgccatccttgcgatcaccattccttgcggcgccggtgctcaacggcct  
 caactactactgggctcctcctaatgcaggagtcgataagggagagcgtcgaccgatgcccttgcgatcaccattccttgcggcgccggtgctcaacggcct  
 atgactatcgtccgcacttatgactgtcttcttcatgcaactcgtaggacaggtgccggcagcgtcctgggtcatttgcggcaggaccgttgcctggagcgga  
 cgatgatcggcctgctccttgcggatcggaaatcgtcacgccctcgtcaagccttgcactgggtcccgccaccaaacgttgcggcagaagcaggccattatcggc  
 gcatggcggccgacgcctgggctactcttgcggcgtcgcgacgcgaggtggatggccttccccattatgattcttgccttccggcggcagcgggatccccgc  
 gttcaggccatgctgtccaggcaggtagatgacgacctaggggacagctcaaggatcgtcggcgtcttaccagcctaacttcgatcattggaccgctgatcgtca  
 cggcattatgccctcggcagcactggaacgggtggcatggattgtagggccgcctataccttctcctccccggttgcgtcgggtgatggagccg  
 ggccacctgacctgaatggaagccggcggcacctcgtaacggatcaccactccaagaattggagccaatcaattcttgcggagaactgtgaatgcgcaaaccaac

ccttggcagaacataatccatcgcgtccgcatctccagcagccgcacggcgcacatctgggcagcgttgggtcctggccacgggtgcatgatcgtctctgctgt  
 tgaggaccgggtaggtgctggcggggtgcttactggttagcagaatgaatcaccgatacgcgagcgaacgtgaagcactgctgctgcaaaacgtctgacactgag  
 caacaacatgaatggtcttccggttctggtttcgttaagcttgaaacgcggaaagtcagcgcctgcaccattatgtccggatctgcatcgcaggatgctgctggctacc  
 ctgtggaacacctacatctgtattaacgaagcgtgacatgacccctgagtgatftttctctggctccgccatccataaccgccagttgttaccctcacaacgttccagtaa  
 ccgggcatgttcatcatcagtaaccgfatcgtgagcatcctctctgfttcatcggtatcattacccccatgaacagaatcccccttacaggaggtcatcagtgaccaaac  
 aggaaaaaaccccttaacatgcccgccttatcagaagccagacattaacgcttctggagaaactaacagctggacgcggatgaacaggcagacatctgtgaatc  
 gcttcacgaccacgctgatgagcttaccgcagctgcctcgcgcttccggtgatgacggtgaaaacctctgacacatgacgctcccggagacggtcacagcttctgtg  
 aagcggatgcccgggagcagacaagcccgtcagggcgcgtcagcgggtgttggcAggtgtcggggcgcagccatgaccagtcacccatggtgcagtgaagg  
 cggcggagccgacaccacggccaccgatattttgcccgatgtacgcgcgctggatgaaCaccagccctcccggctttatcaaaaagagtattgacttaagctaa  
 cctataggatactfacagcgtatggagaggtgtagtgtaaccagaagataagatgcttctgctacctggagagacgcgccgctgatctttgcaatacggccacgc  
 gatggtaacagcttggcgggttctgtaaaactggcagggcgttctgctagatccccgttacaggcggcttctgctgggactgggtggtatcagctgctgataaata  
 atgaaaacggcaaccctgtgtacctcagcaattgtgagcggataacaattcctcagctgctcccctcagcggcccaagaaaactatcccagcccttactgcccctgt  
 ttgaccgctgggatctgtgtaacagagcattagcgaaggtgattttgtcttctgctgctaattttccattgctagatgagcagatagcggagtgatactggttaactat  
 gcggcatcagagcagattgactgagagtgaccatagcgggtgtaataaccgcacagatgcgtaaggagaaaataaccgacagcgccttccgcttctcgtcctac  
 tgactcgtcgcctcggctgctcggcggcagcggatcagctcactcaaaaggcggtaatacggttatccacagaatcaggggataacgcaggaagaacatgtg  
 agcaaaaaggccagcaaaaggccaggaaccgtaaaaaggccgcttctgctggcgttttccataggctcccggcccccctgacgacatcacaataacgacgctcaagta  
 gaggtggcgaaccggacagactataaagataaccagcgtttccccctggaagctccctcgtgctcctctgttccgacctgcccgttaccggatacctgtccgctt  
 tctcccttgggaagcgtggcgttctcctatagctcacgctgtaggtatctcagttcgggtgaggtcgttcccaagctggcctgtgtgacgaacccccgttccagccc  
 gaccgctgcgcttaccggtaactatcgtcttgagtcacaccggtaagacacgacttatcgcactggcagcagccactggtaacaggattagcagagcaggatgt  
 aggcggtgctacagagttctgaagtggtggcctaactacggctacactagaaggacagtatttggatctgcgctcgtctgtaagccagttacccttggaaaaagagttggt  
 agctcttgatccggcaacaacaccgctggtgtagcgggtgtttttgttgcagcagattacgcgcaaaaaaaggatctcaagaagatcctttgatcttttctac  
 ggggtctgacgctcagtggaacgaaaactcagtttaagggattttgtcatgagattatcaaaaaggatcttccactagatccttttaaatataaatgaagtttaaatcaatc  
 taaagtataatagtaaaactgtgctgacagttaccaatgcttaatcagtgaggcacctatctcagcagatctgtctatfttcgttcatccatagttgcctgactccccgtcgtgta  
 gataactacgatacgggagggtaccatctggccccagtgctgcaatgataccgcgagaccacgctaccggctccagattatcagcaataaaccagccagccgg  
 aaggccgagcgcagaagtggtctgcaactttatccgctccatccagctatataattgttgcgggaagctagagtaagtagttgccagtaaatgttgcgcaacgtt  
 gttgccattgctgcagcagcagctggtgtcacgctcgtctgttggatgcttccattcagctccgggttccaacgatcaaggcaggttaccatgatccccatgtgtgcaaaaa  
 agcggttagctcctcgtctccgatcgtgtcagaagtaagttggccgagtggtatcactcatggttatggcagcactgcataattcttactgctatccatccgtaaga  
 tgcctttctgactggtgagactcaaccaagtcattctgagaatagtgatgcggcgaccagttgctcttggccggcgtcaacacgggataataccgcccacatagca  
 gaactttaaaggtctcatcattgaaaacgttcttggggcgaactcctcaagatcttaccgctgttgatccagttcagatgaaccactcgtgcaccaactgatctt  
 cagcatctttacttaccagcgttcttgggtgagcaaaaacaggaaggcaaaatccgcaaaaaagggaataaggcgcacaggaatgtgaaatactatactcttcc  
 ttttcaatattatgaagcattatcagggttattgtctcatgagcggatacatattgaaatgatttagaaaaataaacaataagggttccgcccacatttcccgaaggtgc  
 cacctgacgtctaagaacattatcatgacattaacctataaaaataggcgtatcacaggcccttctgcttcaagaattctcatgtttgacagcttcatcagataagct  
 ttaatcggtagtt

Primer Name	Primer Sequence
A/pDL2317/4536 (Tm = 57)	TGATACCGCGAGACCCAC
A-pUC19-715 (Tm = 56)	GCAGCGAGTCAGTGAGC
A/pZV/4900 (Tm = 55)	AAATCTGGAGCCGGTGAG
S-pDD_1N-3234 (Tm = 55)	ACGCTGTAGGTATCTCAGTTC
A-pUC19-1440 (Tm = 61)	TCTGCGCGTAATCTGCTGCT
S-pDD_1N-2811 (Tm = 56)	ACCGCACAGATGCGTAAG

Appendix B:

```

function varargout = VideoPlayer(varargin)
% VIDEOPLAYER MATLAB code for VideoPlayer.fig
%     VIDEOPLAYER, by itself, creates a new VIDEOPLAYER or raises the existing
%     singleton*.
%
%     H = VIDEOPLAYER returns the handle to a new VIDEOPLAYER or the handle to
%     the existing singleton*.
%
%     VIDEOPLAYER('CALLBACK',hObject,eventData,handles,...) calls the local
%     function named CALLBACK in VIDEOPLAYER.M with the given input arguments.
%
%     VIDEOPLAYER('Property','Value',...) creates a new VIDEOPLAYER or raises the
%     existing singleton*. Starting from the left, property value pairs are
%     applied to the GUI before VideoPlayer_OpeningFcn gets called. An
%     unrecognized property name or invalid value makes property application
%     stop. All inputs are passed to VideoPlayer_OpeningFcn via varargin.
%
%     *See GUI Options on GUIDE's Tools menu. Choose "GUI allows only one
%     instance to run (singleton)".
%
% See also: GUIDE, GUIDATA, GUIHANDLES

% Edit the above text to modify the response to help VideoPlayer

% Last Modified by GUIDE v2.5 26-Mar-2021 00:26:36

% Begin initialization code - DO NOT EDIT
gui_Singleton = 1;
gui_State = struct('gui_Name',       mfilename, ...
                  'gui_Singleton',  gui_Singleton, ...
                  'gui_OpeningFcn', @VideoPlayer_OpeningFcn, ...
                  'gui_OutputFcn',  @VideoPlayer_OutputFcn, ...
                  'gui_LayoutFcn',  [] , ...
                  'gui_Callback',   []);
if nargin && ischar(varargin{1})
    gui_State.gui_Callback = str2func(varargin{1});
end

if nargout
    [varargout{1:nargout}] = gui_mainfcn(gui_State, varargin{:});
else
    gui_mainfcn(gui_State, varargin{:});
end
% End initialization code - DO NOT EDIT

% --- Executes just before VideoPlayer is made visible.
function VideoPlayer_OpeningFcn(hObject, eventdata, handles, varargin)
% This function has no output args, see OutputFcn.
% hObject    handle to figure
% eventdata  reserved - to be defined in a future version of MATLAB
% handles    structure with handles and user data (see GUIDATA)
% varargin   command line arguments to VideoPlayer (see VARARGIN)

% Choose default command line output for VideoPlayer
handles.output = hObject;

% Update handles structure
guidata(hObject, handles);

```

```

% UIWAIT makes VideoPlayer wait for user response (see UIRESUME)w
% uiwait(handles.figure1);

% --- Outputs from this function are returned to the command line.
function varargout = VideoPlayer_OutputFcn(hObject, eventdata, handles)
% varargout  cell array for returning output args (see VARARGOUT);
% hObject    handle to figure
% eventdata  reserved - to be defined in a future version of MATLAB
% handles    structure with handles and user data (see GUIDATA)

% Get default command line output from handles structure
varargout{1} = handles.output;

% --- Executes on button press in LVbutton.
function LVbutton_Callback(hObject, eventdata, handles)
% hObject    handle to LVbutton (see GCBO)
% eventdata  reserved - to be defined in a future version of MATLAB
% handles    structure with handles and user data (see GUIDATA)
% button opens explorer for file selection
[filename, pathname] = uigetfile({'*.mp4'}, 'Selector');
if ~ischar(filename)
    return; %user canceled dialog
end
fullpathname = strcat(pathname,filename);
set(handles.Text1, 'String', fullpathname);

% --- Executes on key press with focus on LVbutton and none of its controls.
function LVbutton_KeyPressFcn(hObject, eventdata, handles)
% hObject    handle to LVbutton (see GCBO)
% eventdata  structure with the following fields (see MATLAB.UI.CONTROL.UICONTROL)
%           Key: name of the key that was pressed, in lower case
%           Character: character interpretation of the key(s) that was pressed
%           Modifier: name(s) of the modifier key(s) (i.e., control, shift) pressed
% handles    structure with handles and user data (see GUIDATA)
% empty

% --- Executes on button press in PlayButton.
function PlayButton_Callback(hObject, eventdata, handles)
% hObject    handle to PlayButton (see GCBO)
% eventdata  reserved - to be defined in a future version of MATLAB
% handles    structure with handles and user data (see GUIDATA)
% begins video playback; when already playing video, restarts it
filename = get(handles.Text1, 'String');

ax = handles.ax1;
obj = VideoReader(filename);
numFrames = 0;

while hasFrame(obj)
    vidFrame = readFrame(obj);
    image(vidFrame, 'Parent', ax);
    set(ax, 'Visible', 'off');
    set(handles.textd, 'String', obj.CurrentTime)
    pause(1/obj.FrameRate);
    numFrames = numFrames + 1;
    set(handles.textf, 'String', numFrames);
end

```

```
clear obj;

% --- Executes on button press in PointButtonA.
function PointButtonA_Callback(hObject, eventdata, handles)
% hObject    handle to PointButtonA (see GCBO)
% eventdata  reserved - to be defined in a future version of MATLAB
% handles    structure with handles and user data (see GUIDATA)
% point A selection and coordinate display
pA = drawpoint;
pA.Label = 'A';
APos = pA.Position;
set(handles.text5, 'String', APos);

% --- Executes on button press in PointButtonB.
function PointButtonB_Callback(hObject, eventdata, handles)
% hObject    handle to PointButtonB (see GCBO)
% eventdata  reserved - to be defined in a future version of MATLAB
% handles    structure with handles and user data (see GUIDATA)
% point B selection and coordinate display
pB = drawpoint;
pB.Label = 'B';
BPos = pB.Position;
set(handles.text6, 'String', BPos);

% --- Executes on button press in PauseButton.
function PauseButton_Callback(hObject, eventdata, handles)
% hObject    handle to PauseButton (see GCBO)
% eventdata  reserved - to be defined in a future version of MATLAB
% handles    structure with handles and user data (see GUIDATA)
% pauses the video
global pauseS
if pauseS==true
    pauseS=false;
else
    pauseS=true;
end
if pauseS == false
    while(1)
        pause(0.001);
        if pauseS == true
            break;
        end
    end
end
end
```

Appendix C:

Protocol as of 2/18/2021

Buffers:

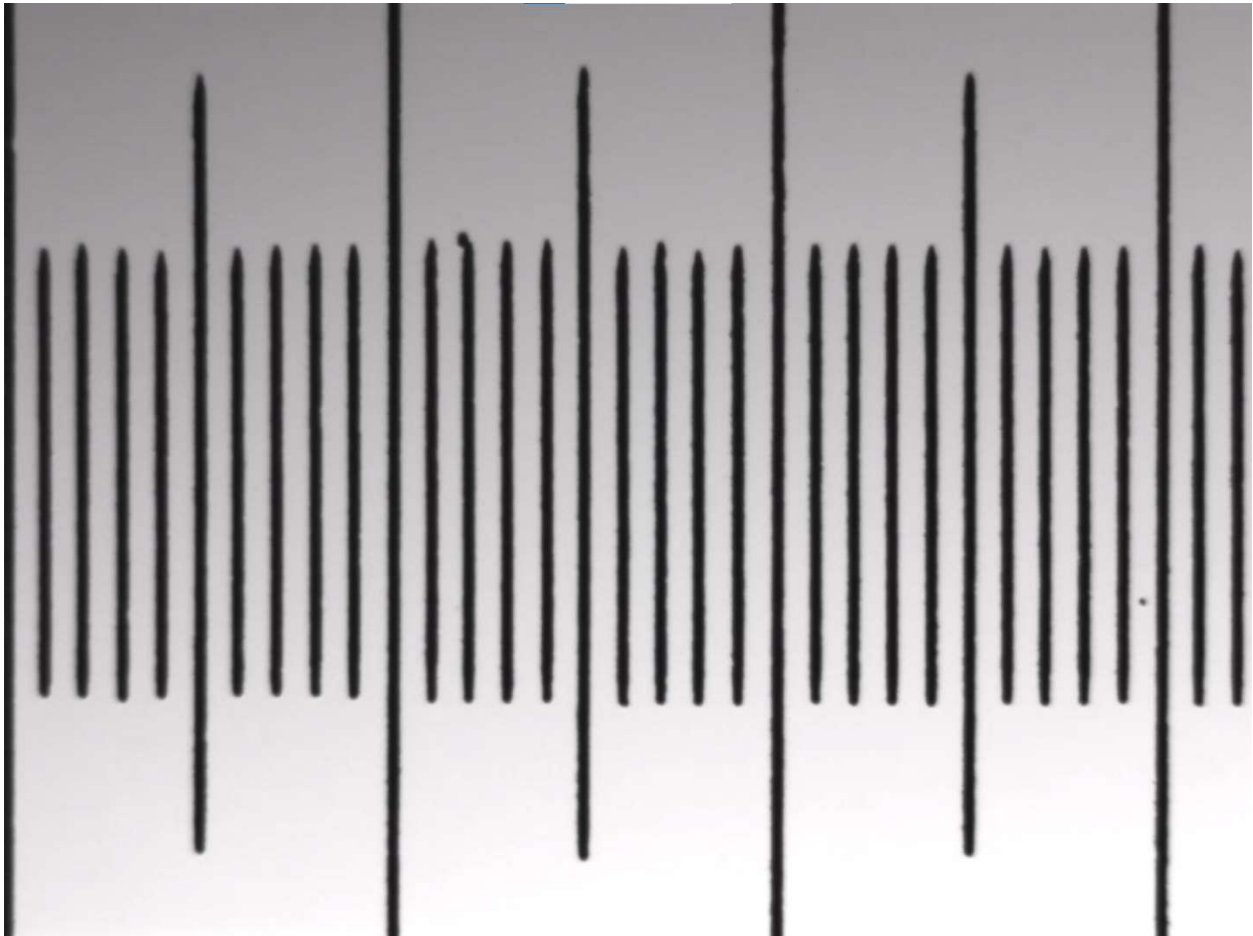
- Phosphate buffered saline, PBS
  - bead wash buffer, BWB (1 M NaCl in TE pH 7.5)
  - tethered bead buffer; TBB (100 mM NaCl in 20 mM Tris-HCl pH 7.5, 1 mM EDTA)
  - stretching buffer, SB (100 mM NaCl w/ 0.2 mg/ml casein w/ 0.5 % Tween in 20 mM Tris-HCl pH 7.4, 2 mM EDTA)
1. Clean regular microscope slides and 24 X 50 No. 1.5 coverslips by oscillating 60 min in lab soap, rinse copiously with H<sub>2</sub>O and dH<sub>2</sub>O, and store under ethanol.
  2. Using the laser cutter, cut parafilm gasket.
  3. Place the gasket on a microscope slide and place a 24 X 50 No. 1.5 coverslip (with a hole drilled in at one end) over the gasket leaving only the end of the entrance well exposed.
  4. Take two small squares of parafilm with holes cut in the middle and place them over the entrance well, making sure to leave the air-water interface that forms between the two glass pieces undisturbed. Take another small parafilm square and place it over the exit well, lining up the hole in the square with the hole in the glass.
  5. Cut a ferrule to the first line and place the ferrule over the two small parafilm squares aligned with the entrance well.
  6. Heat the assembly on a hot plate on a low setting to keep from overheating the parafilm and avoid sputtering as the parafilm melts and adheres to both glass surfaces. Be sure to apply gentle pressure to the coverslip, especially all the way around the exit well, as well as to the top of the ferrule to adhere it to the parafilm, to create a tight seal.
  7. Allow the sealed chamber to cool.
  8. Fill the chamber with 30 ul of 0.2 um filtered PBS by pipetting into the entrance well while wicking solution from the exit well using a twisted tissue.
  9. Draw 25 ul of 4 ug/ml anti-digoxigenin (Roche (2016); in PBS) into the chambers and incubate at 100% relative humidity 1.5-2 hours at room temperature.
  10. Vortex gently to resuspend MyOne (Invitrogen) beads and dilute 1 ul of beads in 150 ul of BWB in a 1.5 ml microcentrifuge tube. Mix well by flicking.
  11. Place against magnet for 5 min.; Remove the solution; Resuspend in 150 ul of BWB.
  12. Place against magnet for 5 min.; Remove the solution; Resuspend in 150 ul of TBB.
  13. Place against magnet for 5 min.; Remove the solution; Resuspend in 100 ul of TBB.
  14. Add 10 ul ligation reaction to 30 ul TBB. Flick gently to mix 4x dilution.
  15. Add 15 ul of TBB microsphere resuspension and incubate for 15 mins.
  16. Gently rinse the microchambers with 30 ul of SB and incubate for at least 5 min to passivate any exposed glass in the chamber.
  17. Spike the 4X bead-DNA solution with 3 ul of 0.1 uM d-biotin (Sigma) in TE, mix, and incubate for 5 min.
  18. Place microchamber on slide adapter. Make sure to align the exit well with the opening of the blue ferrule. Do not tighten excessively, as the coverslip is prone to cracking and the seal will break. Place the slide adapter with the microchamber on the microscope for observation.
  19. Use the microscope software to find and focus on the parafilm gasket. (Between +30 and -90 is where it usually focuses)
  20. Load 30 ul of bead-DNA solution into the entrance well. Using the pump, introduce the DNA tethers at no faster than 300 ul/hr on the settings. Let sit for at least 10 minutes.
  21. After 5 min. gently rinse the microchamber with 30 ul of SB.

## Previous Protocol (From 04/2019)

## Buffers:

- Phosphate buffered saline, PBS
- bead wash buffer, BWB (1 M NaCl in TE pH 7.5)
- tethered bead buffer; TBB (100 mM NaCl in 20 mM Tris-HCl pH 7.5, 1 mM EDTA)
- stretching buffer, SB (100 mM NaCl w/ 0.2 mg/ml casein w/ 0.5 % Tween in 20 mM Tris-HCl pH 7.4, 2 mM EDTA)

1. Clean 24 X 40 and 22 X 22 No. 1.5 coverslips by oscillating 60 min in lab soap, rinse copiously with H<sub>2</sub>O and dH<sub>2</sub>O, and store under ethanol.
2. Using the laser cutter, cut a parafilm gasket to create three serpentine channels (not shown).
3. Place the gasket on a 24 X 50 coverslip and place a 22 X 22 No. 1.5 coverslip on the gasket leaving only the ends of the channels exposed.
4. Heat the assembly on a hot plate on a low setting to keep from overheating the parafilm and avoid sputtering as the parafilm melts and adheres to both glass surfaces. Gentle pressure applied using another microscope slide or forceps helps sealing.
5. Allow the sealed chamber to cool.
6. Fill the chamber with 15 ul of 0.2 um filtered PBS by pipetting into the entrance well while wicking solution from the exit well using a twisted tissue.
7. Draw 15 ul of 4 ug/ml anti-digoxigenin (Roche (2016); in PBS) into the chambers and incubate at 100% relative humidity overnight at 4 °C.
8. Vortex gently to resuspend MyOne (Invitrogen) beads and dilute 3 ul of beads in 147 ul of BWB in a 1.5 ml microcentrifuge tube. Mix well by flicking.
9. Place against magnet for 5 min.; Remove the solution; Resuspend in 150 ul of BWB; repeat once
10. Add 300 ul of Nanopure H<sub>2</sub>O.
11. Split into 150 and 300 ul aliquots
12. Place against the magnet for 5 min; Remove the solutions; Resuspend the 150 ul “stuck” aliquot in 300 ul of 0.2 micron filtered PBS; Resuspend the 300 ul “tether” aliquot in 200 ul of TBB.
13. Introduce 15 ul “stuck” aliquots into the chambers and incubate in a humid box for at least 10 min.
14. Add 10 ul of a ligation reaction (guess 12 fmol) to 10 ul of TBB in 0.65 ml microcentrifuge tube and pipet/flick this 2X dilution gently to mix. Add 10 ul of this to 10 ul of TBB in 0.65 ml microcentrifuge tube and pipet/flick this 4X dilution gently to mix. Add 10 ul of this to 10 ul of TBB in 0.65 ml microcentrifuge tube and pipet/flick this 8X dilution gently to mix.
15. Mix 10 ul of the dilutions of ligations with 10 ul of the corresponding microsphere resuspensions in 0.65 ml microcentrifuge tubes and incubate for 15 minutes.
16. Gently rinse the microchambers with 30 ul of SB and incubate for at least 5 min to passivate any exposed glass in the chamber.
17. Spike the bead-DNA solutions with 1 ul of 0.1 uM d-biotin (Sigma) in TE, mix, and incubate for 5 min.
18. Gently introduce 15 ul of the bead-DNA solution into the microchamber.
19. After 5 min. gently rinse the microchamber with 30 ul of SB.
20. Place on the microscope for observation

Appendix D:

1 mm calibration slide with .01 mm divisions.

32 lines x .01 mm = 0.32 mm or 320 microns

Image  $w \times h = 1392 \times 1040$  pixels

1392 pixels / 320 microns = 4.35 pixels/micron or 0.2299 microns/pixel